Stem Cell Reports
Article
ISSCR
OPEN ACCESS

Novel Lineage-Tracing System to Identify Site-Specific Ectopic Bone Precursor Cells

Chase A. Pagani,[1] Amanda K. Huber,[2] Charles Hwang,[2] Simone Marini,[2] Karthik Padmanabhan,[3] Nicholas Livingston,[1] Johanna Nunez,[1] Yuxiao Sun,[1] Nicole Edwards,[2] Yu-Hao Cheng,[4] Noelle Visser,[2] Pauline Yu,[2] Nicole Patel,[2] Joseph A. Greenstein,[2] Husain Rasheed,[2] Reagan Nelson,[2] Karen Kessel,[2] Kaetlin Vasquez,[2] Amy L. Strong,[2] Geoffrey E. Hespe,[2] Jane Y. Song,[5] Deneen M. Wellik,[5] and Benjamin Levi[1,*]
[1]Center for Organogenesis and Trauma, Department of Surgery, University of Texas Southwestern, 6000 Harry Hines Boulevard, Dallas, TX 75235, USA
[2]Section of Plastic Surgery, Department of Surgery, University of Michigan, Ann Arbor, MI 48109, USA
[3]BRCF Epigenomics Core, University of Michigan, Ann Arbor, MI 48109, USA
[4]Institute for Cell Engineering, Johns Hopkins School of Medicine, Baltimore, MD 21205, USA
[5]Department of Cell and Regenerative Biology, University of Wisconsin, Madison, WI 53705, USA
*Correspondence: benjamin.levi@utsouthwestern.edu
https://doi.org/10.1016/j.stemcr.2021.01.011

SUMMARY

Heterotopic ossification (HO) is a form of pathological cell-fate change of mesenchymal stem/precursor cells (MSCs) that occurs following traumatic injury, limiting range of motion in extremities and causing pain. MSCs have been shown to differentiate to form bone; however, their lineage and aberrant processes after trauma are not well understood. Utilizing a well-established mouse HO model and inducible lineage-tracing mouse (*Hoxa11*-CreER^{T2};*ROSA26-LSL-TdTomato*), we found that *Hoxa11*-lineage cells represent HO progenitors specifically in the zeugopod. Bioinformatic single-cell transcriptomic and epigenomic analyses showed *Hoxa11*-lineage cells are regionally restricted mesenchymal cells that, after injury, gain the potential to undergo differentiation toward chondrocytes, osteoblasts, and adipocytes. This study identifies *Hoxa11*-lineage cells as zeugopod-specific ectopic bone progenitors and elucidates the fate specification and multipotency that mesenchymal cells acquire after injury. Furthermore, this highlights homeobox patterning genes as useful tools to trace region-specific progenitors and enable location-specific gene deletion.

INTRODUCTION

The correct programming of adult precursor cells is critical to enable normal wound healing after injury. Burn injuries, soft-tissue wounds, and fractures all require a highly orchestrated response of inflammatory, vascular, neural, fibroblast, and mesenchymal stem/progenitor/precursor cells (MSCs) to coordinate proper healing. However, in some cases of severe trauma, proper precursor cell programming can be maladaptive, causing pathological healing. This altered programming of precursor cells is manifested in the process of heterotopic ossification (HO). HO is characterized by aberrant differentiation of adult tissue-resident MSCs that are ectopic from the adult skeleton. Recent studies have begun to elucidate bone progenitor cells during normal bone development and repair. The process by which tissue-resident mesenchymal cells undergo aberrant osteogenic and chondrogenic differentiation, however, has yet to be defined (Agarwal et al., 2016a, 2017a; Chan et al., 2018; Comazzetto et al., 2019; Genet et al., 2015; Hsieh et al., 2019; Hwang et al., 2019; Matsushita et al., 2020; Torossian et al., 2017; Wang et al., 2018).

In recent years, Cre/LoxP-based lineage-tracing approaches have provided the technical ability to follow the fates of stably marked native cell populations within the injury site and assess these cells' osteogenic capacity (Agarwal et al., 2016a; Kan et al., 2018). Although lineage studies have characterized HO as an endochondral process (Foley et al., 2018), studies have yet to elucidate whether several cell populations differentiate into aberrant cartilage and bone or whether HO is derived from one progenitor population. Mouse lines that mark local MSCs have been used to study HO (Agarwal et al., 2016b, 2017b; Dey et al., 2016; Kan et al., 2013, 2018). However, these Cre models have limitations. For example, *Prrx1Cre* marks the entire lateral plate mesoderm, and each Cre allele is found at many sites outside of the musculoskeletal system (Logan et al., 2002). Given the lack of specificity, use of these Cre systems will not precisely identify the cells likely playing a role in bone formation or in homeostasis (Agarwal et al., 2016a). Cre systems have also been used to conditionally delete genes during development; however, this can lead to native skeletal abnormalities such as shortened limbs or altered bone mineral density, introducing confounding variables into the measurement of ectopic bone. Therefore, inducible systems are preferred. The available alleles that mark MSCs include *PdgfraCreER*, *Gli1CreER*, and *ScxCreER* lines; however, these alleles also mark MSCs in tissues outside of the extremities (Li et al., 2018; O'Rourke et al., 2016; Qian et al., 2017; Sugimoto et al., 2013b; Zhao et al., 2015). Importantly, these cell lineages are not specific to one anatomic region, making it difficult to interpret any lineage specific gene-deletion studies.

Recent studies have utilized the embryonic patterning gene *Hoxa11* to mark the progenitor cells responsible for

fracture healing (Pineault et al., 2019). MSCs are mesoderm-derived and *Hox* genes have been shown to be expressed in a region-specific manner in these cells (Pineault et al., 2019). *Hoxa11* is expressed specifically in the zeugopod, the radius-ulna and tibia-fibula region of the limb. *Hoxa11-CreER^{T2};ROSA26-LSL-TdTomato* lineage-trace reporter mouse model marks *Hoxa11*-lineage cells during skeletal development and growth. At 24 h following tamoxifen induction at postnatal day 3, *Hoxa11*-lineage cells are found within perichondrium at the distal growth plate, periosteal, endosteal, and trabecular bone surfaces. After 8 weeks, these cells are found in the periosteum, endosteum, and bone marrow space (Pineault et al., 2019). However, *Hoxa11*-expressing cells are not isolated to the skeleton. It was found that *Hoxa11* cells expressing endogenous GFP are located in tendon and muscle interstitial tissue at embryonic day 14.5, yet it remains unclear whether these cells persist in the adult tendon and muscle (Pineault et al., 2019). Furthermore, using *Hoxa11-CreER^{T2};ROSA26-LSL-TdTomato* mice, it was shown that *TdTomato*$^{+}$ (*Hoxa11*iTom^{+}) MSCs were marked prior to *Sox9CreER* and *OsxCreER* lineage-marked cells, indicating that these *Hoxa11*-expressing cells serve as progenitors for osteoblastogenesis and chondrogenesis (Pineault et al., 2019). These results suggest that *Hoxa11* marks the primitive MSCs that may be responsible for the formation of aberrant ectopic bone.

In the current study, we utilize a burn/tenotomy (BT) injury model in *Hoxa11-CreER^{T2};ROSA-LSL-TdTomato* mice to identify, lineage trace, and analyze the cell fate of the HO progenitor cells. This model reproducibly results in HO formation, which allows for the evaluation of the precursor cells responsible for aberrant bone formation. Using single-cell RNA sequencing (scRNA-seq) and single-nucleus assay for transposase-accessible chromatin using sequencing (snATAC-seq), we were able to specifically identify and analyze MSCs marked by *TdTomato* transcript and MSCs not marked by *TdTomato*. We found that *TdTomato*-expressing MSCs were also identified by markers of chondrocytes and osteoblasts. Using trajectory analyses, we identify the *TdTomato*$^{+}$ population responsible for chondrogenic and osteogenic differentiation. Our findings also suggest that these cells can differentiate into adipocytes following injury. Our results demonstrate that *Hoxa11*-lineage cells are a unique population of precursor cells that undergo an aberrant fate change toward a chondrogenic and osteogenic cell type.

RESULTS

Hoxa11-lineage cells express genes associated with mesenchymal cells at baseline and after injury

To characterize the cells at the HO site, we performed scRNA-seq on cells harvested from the distal hindlimb of an uninjured mouse, injured left hindlimb 1 week after BT injury, and injured hindlimb 6 weeks after BT injury of *Hoxa11-CreER^{T2};ROSA-LSL-TdTomato* mice to determine dynamic molecular changes in the *Hoxa11*-lineage cells (Figure 1A). Specifically, the Achilles' tendon and surrounding soft tissue posterior to the tibia and fibula were harvested (Figure 1A). Native bone, such as the tibia, fibula, tarsals, metatarsals, and phalanges, were not harvested for analysis. Twenty-five unique clusters were created by UMAP analysis. Clusters were identified by uniquely expressed upregulated genes (Figure 1B and Table S1). Cell-cycle phase, G_2/M score, and S score were calculated (Tirosh et al., 2016) (Figure S1A). Because we used *Hoxa11-CreER^{T2};ROSA-LSL-TdTomato* mice, expression of the *TdTomato* RNA transcript was used to identify clusters of the *Hoxa11* lineage. Combined analysis of all conditions and time points identified the following clusters as *TdTomato* expressing: MSC:0, SkMusc:6, MSC:14, and Teno:16 (Figure 1C). Following individual time-point analysis, cluster MSC:2 also showed *TdTomato* expression at the 6-week time point (Figure 1C). These five clusters were the focus of our study due to their expression of the *TdTomato* transcript marking them as *Hoxa11*-lineage cells. Additional genes frequently used to study bone progenitors were included for comparison. SkMusc:6 showed no expression of bone progenitor lineage markers. *Pdgfra* and *Prrx1* mark mesenchymal progenitor cells (Miwa and Era, 2018), and were expressed by clusters MSC:0, MSC:2, MSC:14, and Teno:16 (Figure 1D). *Clec11a*, which has known roles in osteogenic differentiation and bone fracture healing (Yue et al., 2016), was also expressed in clusters MSC:0, MSC:2, MSC:14, and Teno:16 (Figure 1D). *Cxcl12*, a marker commonly used for hematopoietic stem cells (Ding and Morrison, 2013) and osteoblasts (Shahnazari et al., 2013), was expressed in clusters MSC:0, MSC:2, MSC:14, and Teno:16 (Figure 1D). *Clec3b*, previously shown to be important in mineralization (Iba et al., 2001), was expressed in MSC:0, MSC:2, and MSC:14 (Figure 1D). Of the *Hoxa11* lineage clusters, only MSC:14 displayed *Lepr* expression (Figure 1D). *Lepr* encodes the leptin receptor and is frequently used as a marker for bone marrow mesenchymal stem cells (Zhou et al., 2014), suggesting that the MSC:14 cells are of bone origin (Figure 1D). *En1*, which is important in cranial morphogenesis and calvarial defect healing (Deckelbaum et al., 2012), showed expression in MSC:0 and MSC:14 (Figure 1D). Interestingly, *Gli1*, a marker found to be important in bone fracture healing (Shi et al., 2017), showed no expression in *TdTomato*-expressing clusters in the combined time-point analysis (Figure 1D). Lastly, two markers that have been used to mark multipotent skeletal stem cells in humans, *Pdpn* and *Cd164*, were expressed in MSC:0, MSC:2, MSC:14, and Teno:16 (Chan et al., 2018; Walmsley et al., 2015) (Figure 1D). These findings suggest

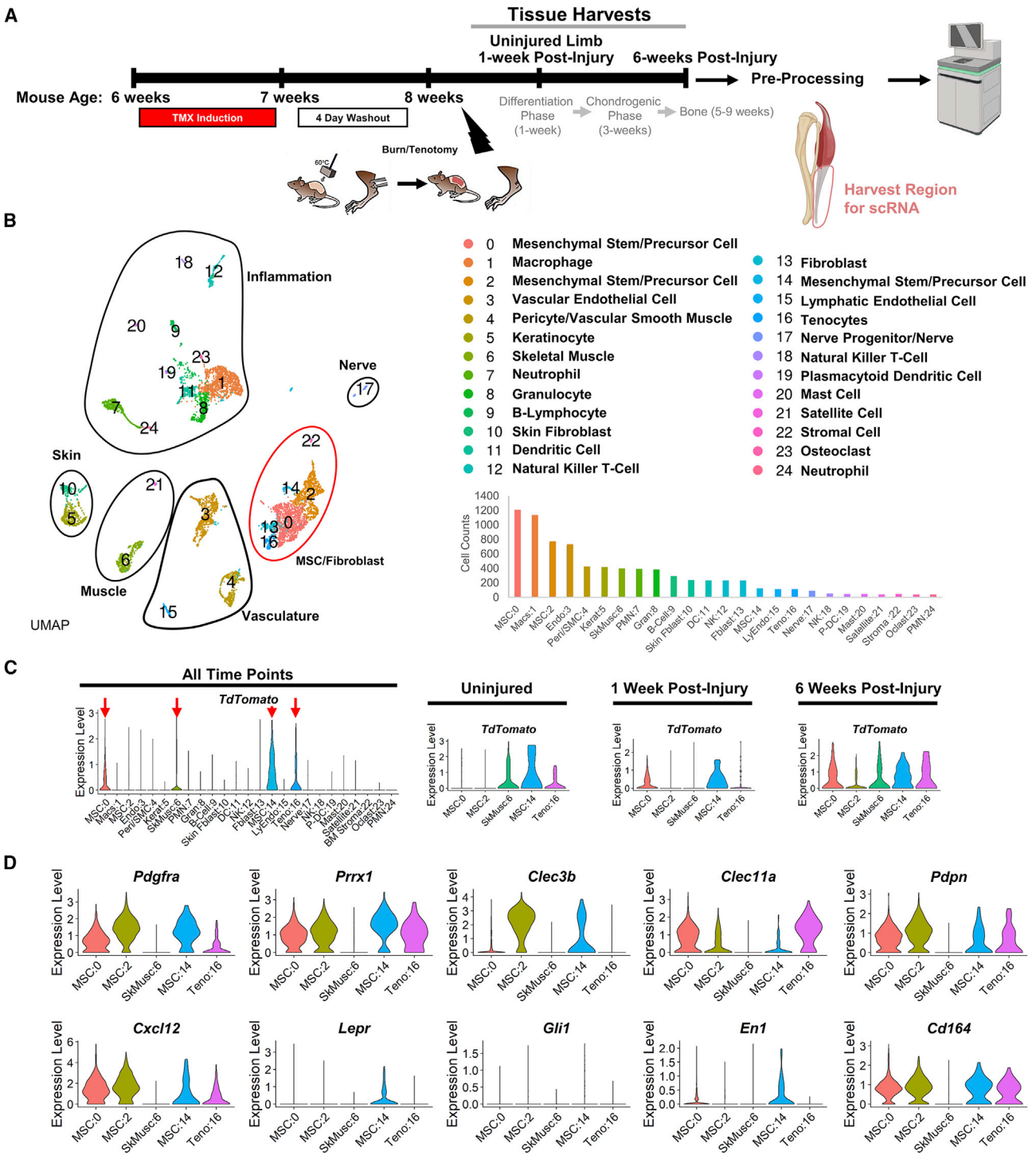

Figure 1. Combined time-point analysis of scRNA sequencing shows distinct TdTomato-expressing clusters

(A) Experimental schematic showing injury model and cells harvested in the uninjured limb (n = 1), 1 week following BT injury (n = 1), and 6 weeks following BT injury (n = 2) from *Hoxa11*-CreER^{T2}:ROSA-TdTomato mice that were processed and sequenced. Mouse schematic adapted from our group's previous work (Agarwal et al., 2016a).

(B) UMAP cluster, cluster definitions, and cell counts of combined time-point analysis.

(C) Violin plots of combined time-point and individual time-point *TdTomato* expression.

(D) Violin plots of gene markers for mesenchymal and bone progenitors.

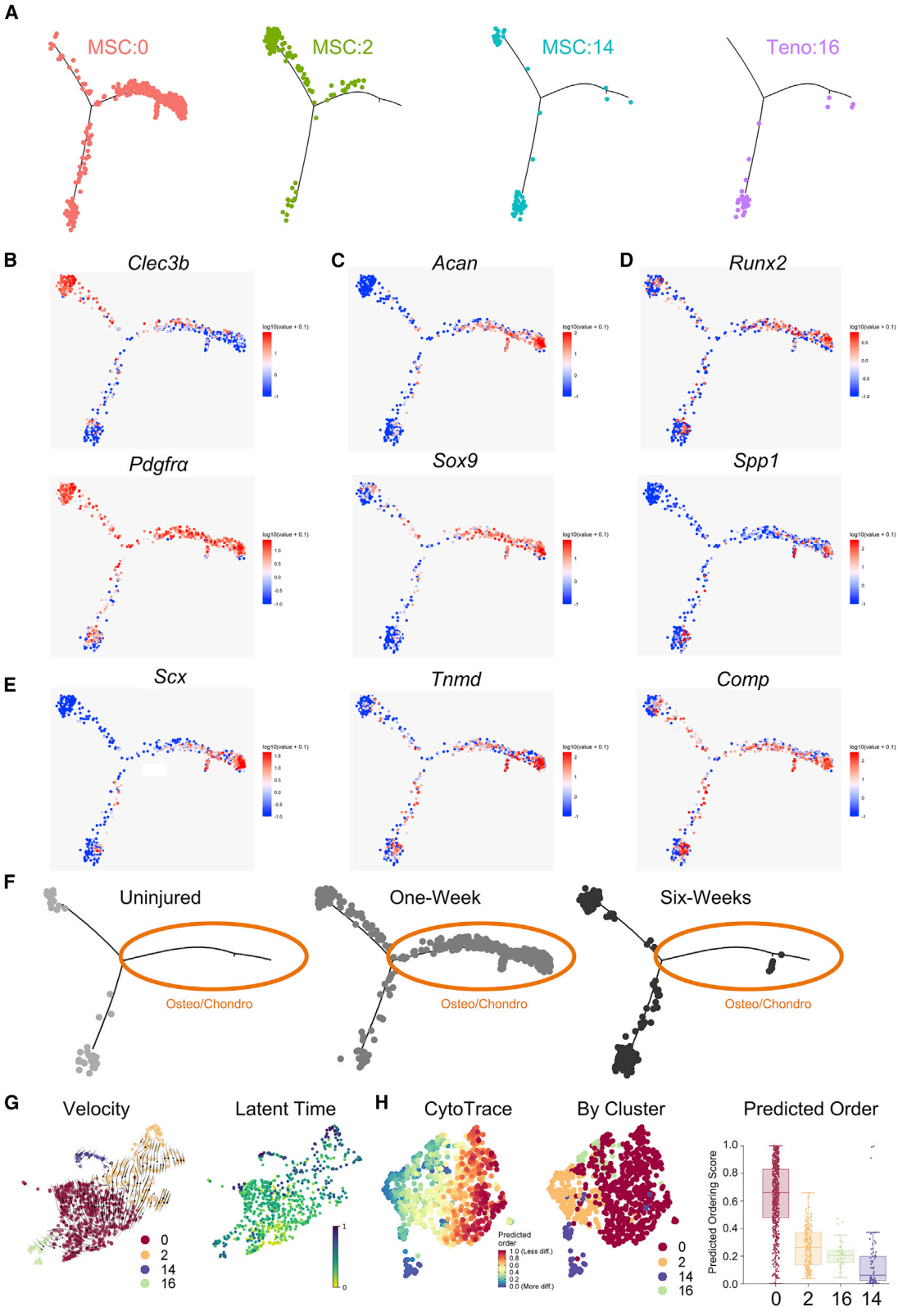

(legend on next page)

that *Hoxa11*-lineage cells may be responsible for forming ectopic bone following injury; however, it remains unclear how these cells progress from normal physiology toward an aberrant cell fate.

Hoxa11-lineage cells turn on transcriptional profiles associated with osteogenic and chondrogenic cell states during HO progression

Following initial scRNA-seq analyses, pseudo-time analysis was used to determine how the transcriptional profiles of *Hoxa11*-lineage cells were changing across the conditions and time points (uninjured, 1 week, and 6 weeks). Cells expressing over at least one count of the *TdTomato* transcript within the four mesenchymal *TdTomato*-expressing clusters were used for pseudo-time analyses (Figure 2A). SkMusc:6 was excluded from the analysis as it formed a separate trajectory (Figure S2). Three major branches were identified by visualizing gene expression across the trajectory: a precursor-like state characterized by *Pdgfra* and *Clec3b* (Figure 2B), a combined osteogenesis/chondrogenesis-like state characterized by bone (*Spp1*, *Runx2*), chondrocyte (*Sox9*, *Acan*), and tenocyte (*Scx*, *Tnmd*) differentiation markers (Figures 2C–2E), and lastly, a branch characterized by tendon markers *Scx*, *Tnmd*, and *Comp* (Figure 2E). Interestingly, *Pdgfra* expression is maintained in the osteo/chondro branch of the analysis. Tendon markers *Scx*, *Tnmd*, and *Comp* are expressed in the osteo/chondro branch, suggesting the *Hoxa11*-lineage cells that comprise HO have tendon origin, which is consistent with previous work (Agarwal et al., 2017b). Importantly, cluster MSC:0 was the only cluster that occupies the terminal end of the osteo/chondro branch (Figure 2A), suggesting that this unique cluster of cells differentiates into heterotopic bone. *Acan* and *Fbn2* were uniquely and highly expressed in MSC:0. Confocal microscopy images showed co-localization of TdTomato fluorophore with ACAN and FBN2 protein in the HO anlagen 1 week following injury (Figure S3). When the trajectory was separated by time after injury, there were no cells occupying the osteo/chondro branch in the uninjured sample, while many cells occupied this branch of the analysis 1 week post injury. A small population, which occupied a small separate branch on the trajectory, remained at 6 weeks (Figure 2F). Few cells are likely found at the 6-week time point as they are entrapped in HO bone and difficult to isolate for scRNA-seq. This dynamic analysis highlights that *Hoxa11*-lineage cells express osteogenic and chondrogenic gene differentiation markers only after injury (Figure 2F).

To delineate the lineage kinetics in the MSCs, we performed trajectory analysis using the estimated RNA velocity of *TdTomato*-positive cells in clusters MSC:0, MSC:2, MSC:14, and Teno:16 (La Manno et al., 2018; Bergen et al., 2020) (Figure 2H). The vectors of individual estimated velocity indicated the origin as cluster MSC:0 with a dual outflow toward MSC:2 and Teno:16. Moreover, there was a minor bifurcation in MSC:2 that pointed toward MSC:14 (Figure 2H). We further inferred the position of cells in the fate commitment process by computing the latent time. The results showed a comparable origin in MSC:0 with four distinct endpoints terminated in MSC:0, MSC:2, MSC:14, and Teno:16 (Figure 2H). Cell-cycle scores, feature counts, and RNA counts were also visualized on the trajectory (Figure S1B). RNA features increased along the right branch of the trajectory. CytoTrace is a trajectory analysis that considers variations in RNA features as a factor in determining differentiation state (Gulati et al., 2020). MSC:0 was the least differentiated compared with other MSC clusters based on CytoTrace predicted ordering (Figure 2H). When taken together, velocity, CytoTrace, and pseudo-time analyses suggest that MSC:0 is able to differentiate into chondrogenic and osteogenic lineages compared with more differentiated MSC:2, MSC:14, and Teno:16 clusters.

To provide a clearer picture of how *Hoxa11*-lineage cells transition throughout the progression of HO, we utilized individual time-point analyses of snATAC, scRNA, and immunofluorescence (IF) microscopy.

Hoxa11-lineage cells do not express markers of osteogenesis or chondrogenesis in uninjured leg

snATAC was utilized to characterize the chromatin states of genes important in chondrogenic and osteogenic

Figure 2. Trajectory analysis of *TdTomato*$^+$ cells shows osteo/chondro branch following traumatic injury

(A) Monocle 2 pseudo-time analysis separated by *TdTomato*-expressing cluster.

(B) Feature plots of *Pdgfra* and *Clec3b* gene expression levels.

(C) Feature plots of chondrocyte differentiation genes *Acan* and *Sox9* expression levels.

(D) Feature plots of osteoblast differentiation genes *Runx2* and *Spp1* expression levels.

(E) Feature plots of tendon differentiation genes *Scx*, *Tnmd*, and *Comp* expression levels.

(F) Pseudo-time plots separated by time point with osteo/chondro branch circled in orange.

(G) UMAP steam plot of RNA velocity of TdTomato$^+$ cells in clusters MSC:0, MSC:2, MSC:14, and Teno:16 (left) with arrows showing velocity and UMAP latent time plot (right).

(H) CytoTrace analysis of *TdTomato*-expressing cells including a UMAP plot with predicted ordering score (left), a UMAP plot colored by cluster (center), and a box plot showing predicted score of clusters (right).

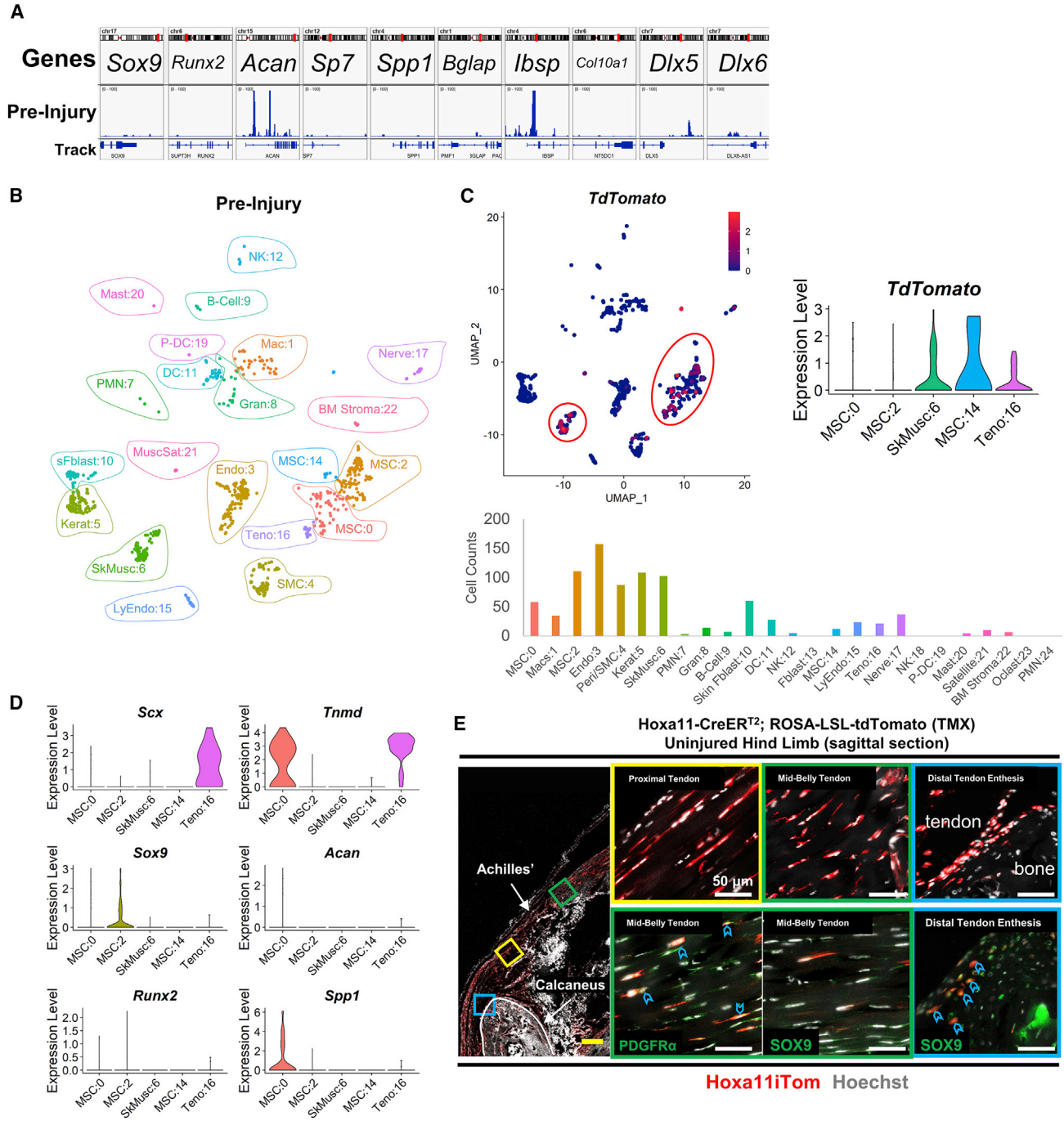

Figure 3. *Hoxa11*-lineage cells are found within tendon and enthesis and do not express chondro/osteo differentiation genes in the uninjured limb

(A) SnATAC-seq of *TdTomato*-expressing cluster MSC:0 in the uninjured limb (n = 1). Genes shown are important in chondrogenesis and osteogenesis. Bars represent mean value of reads.

(B) UMAP plot of cells in the uninjured limb.

(C) UMAP feature plot depicting *TdTomato* expression in the uninjured limb (top left), violin plot showing *TdTomato* expression across clusters (top right, from Figure 1C), and cell counts across all clusters (bottom).

(legend continued on next page)

differentiation. Euchromatin, or "open" chromatin, is important for the transcription of gene loci. snATAC is specifically useful for isolating unique clusters of cells mapped from the scRNA-seq—a technique not available to bulk ATAC. Cluster MSC:0 was the focus of snATAC-seq as this cluster likely contains the cells that differentiate into HO, based on genetic expression at the 1-week post-injury time point. MSC:0 cells showed very low levels of open chromatin reads near promoters of genes important in chondrogenesis and osteogenesis in the uninjured limb (Figure 3A). Chondrogenic gene *Sox9* had a low number of open chromatin reads near promoter regions, suggesting decreased expression (Figure 3A). Chondrogenic gene *Acan* had a higher level of open chromatin reads; however, it was not expressed in scRNA-seq data (Figures 3A and 3D). Genes *Dlx5* and *Dlx6*, which are critical in mammalian skeletal development (Robledo et al., 2002), and *Runx2* had low levels of open chromatin regions (Figure 3A). Later-stage osteoblast differentiation genes *Sp7* and *Spp1* (Komori, 2006, 2017) also had low levels of open chromatin reads. Cells of MSC:0 showed open chromatin regions within and surrounding bone matrix protein-encoding gene *Ibsp*, but not *Bglap* (Komori, 2010) (Figure 3A). As open chromatin is integral for the transcription of genes, this suggests that in the uninjured limb *Hoxa11*-lineage cells are not primed to differentiate toward chondrocytes and osteoblasts. While useful, accessibility to open promoter regions is not the only determinant of gene transcription (Chereji et al., 2019). To account for this, we also characterized the *Hoxa11*-lineage cells in an uninjured limb by analyzing the scRNA transcriptome profiles of *Hoxa11*-lineage clusters and IF data.

We found that the majority of *TdTomato* expression was limited to SkMusc:6, MSC:14, and Teno:16, while MSC:0 and MSC:2 showed minimal expression (Figures 3B and 3C). *Scx* expression was only expressed in Teno:16, while *Tnmd* expression was expressed in both MSC:0 and Teno:16. *Scx* regulates *Tnmd* expression (Shukunami et al., 2018), which suggested that in the uninjured limb, Teno:16 was more stem in nature. Chondrogenic and osteogenic genes showed little to no expression within *Hoxa11*-lineage clusters in the uninjured limb (Figure 3D). These findings suggest that in the uninjured limb, *Hoxa11*-lineage cells are within tendon and muscle but are not primed for aberrant osteogenic and chondrogenic cell fate.

The location and expression of *Hoxa11*-lineage marking by the TdTomato fluorophore was confirmed by confocal microscopy (Figure 3E). *TdTomato* expression was limited to the limb zeugopod following BT injury (Figure S4). Expression was found throughout the Achilles' tendon as well as at the tendon enthesis. IF labeling of mesenchymal progenitor cell marker PDGFRα showed co-localization of TdTomato within the Achilles' tendon. Histological sections were also immunolabeled by SOX9, which only showed expression at the tendon enthesis, not the mid-belly tendon (Figure 3E), which is consistent with previous studies (Sugimoto et al., 2013a). SOX9 immunolabeling also co-localized with *TdTomato*$^+$ cells at the tendon enthesis.

Hoxa11-lineage cells within tendon enter an osteogenic and chondrogenic state following injury

To delineate the gene expression changes after injury, we analyzed snATAC data and scRNA data of the 1-week post-injury cells in the *TdTomato*-expressing cluster MSC:0 (Figures 4A and 4B). SnATAC showed increased levels of open chromatin at chondrogenic genes *Sox9*, *Acan*, and *Col10a1* (Figure 4A). Osteogenic differentiation genes *Runx2*, *Sp7*, *Bglap*, *Ibsp*, *Spp1*, *Dlx5*, and *Dlx6* all showed increased levels of open chromatin reads (Figure 4A). In the scRNA data, *TdTomato* expression was altered following injury, expressed mainly in clusters MSC:0, MSC:14, and at very low levels in Teno:16 (Figure 4C). MSC:0 was characterized by *Scx*, *Tnmd*, *Sox9*, *Acan*, *Runx2*, and *Spp1* (Figure 4D). There was no difference in *Sox9* expression in MSC:2 between the uninjured and injured hindlimb. Interestingly, osteogenic differentiation markers showed increased expression in MSC:14 and Teno:16 following injury (Figure 4D).

Cells were also scored by their expression of *Sox9*, *Runx2*, both *Sox9* and *Runx2*, or neither, to determine whether cells in MSC:0 are undergoing an endochondral ossification process whereby chondrocytes are formed first, which are replaced by osteoblasts, or whether the cells are differentiating directly toward osteoblasts, a process more commonly found in intramembranous bone formation. Of all *TdTomato*$^+$ MSC:0 cells at the 1-week time point (N = 479), 7% expressed only *Runx2* (n = 32), 47% expressed both *Sox9* and *Runx2* (n = 226), 39% expressed only *Sox9* (n = 185), and 8% had no expression of either (n = 36) (Figure 4E). This suggests that a small percentage of the cells within this cluster differentiate directly toward osteoblasts by the 1-week time point and contribute to HO through

(D) Violin plots of genes necessary in differentiation of tenocytes (top), chondrocytes (middle), and osteoblasts (bottom).
(E) Confocal microscopy images of the uninjured hindlimb with tile scan (left) and 63× total zoom inset images of regions of interest (n = 2 mice/antigen of interest, n = 3 images/mouse). Colored boxes in tile show region of inset. Sections were immunolabeled with PDGFRα and SOX9 (bottom). Blue chevrons mark *Hoxa11*iTom cells co-labeled with specified antibodies. Yellow scale bar, 500 μm; white scale bars, 50 μm.

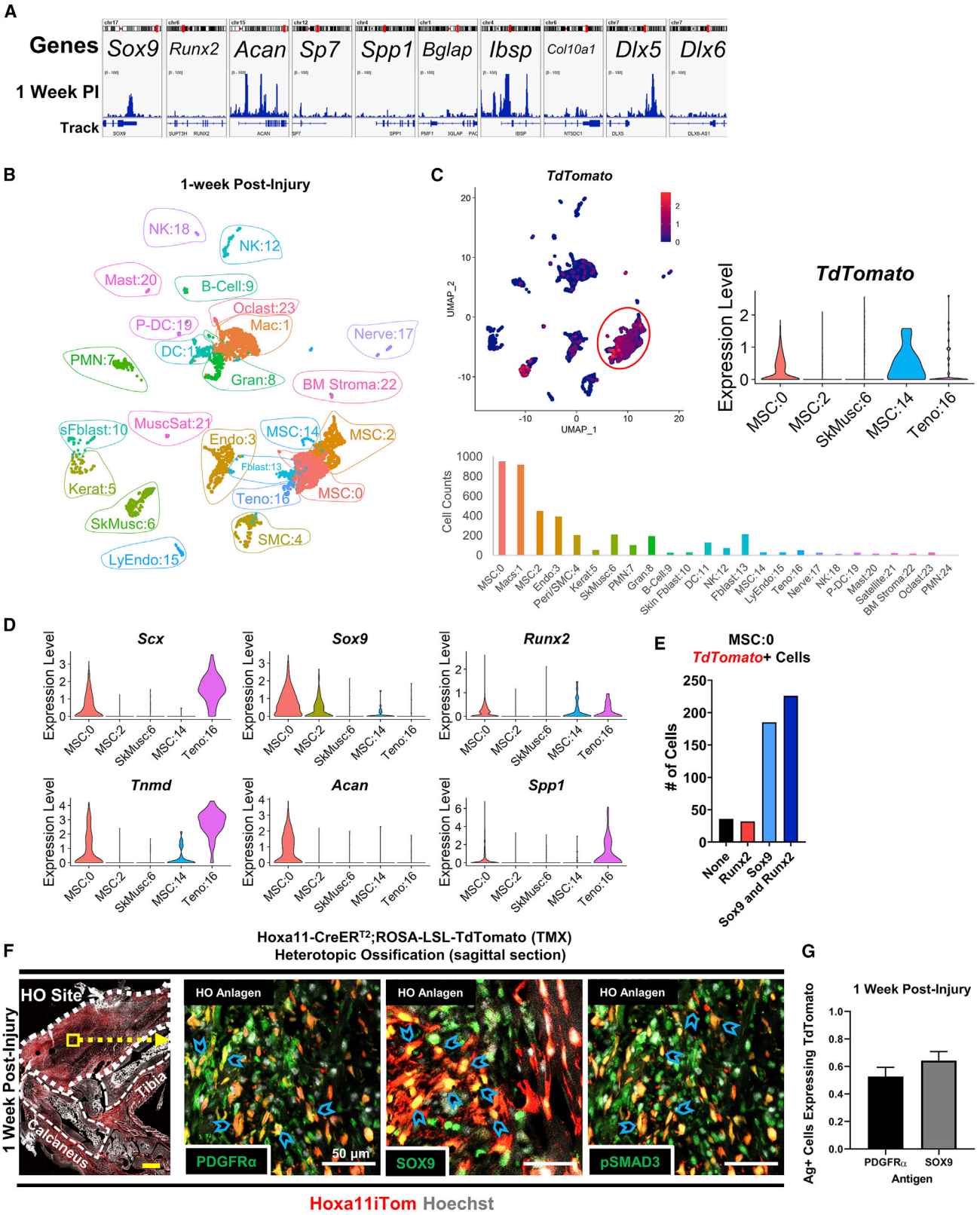

(legend on next page)

intramembranous ossification, while the remaining cells progress through endochondral ossification.

IF labeling of PDGFRα, SOX9, and pSMAD3, signal transducer of the canonical transforming growth factor-β pathway that is critical for HO formation (Sorkin et al., 2020; Wang et al., 2018), was performed within the HO anlagen at the injury site at the 1-week time point. All antigens showed co-localization with TdTomato fluorophore marking the *Hoxa11*-lineage cells (Figure 4F). PDGFRα$^+$ TDTOMATO$^+$ cells showed elongated morphology, suggesting a predifferentiated state, while SOX9$^+$ *TdTomato*$^+$ cells had rounded, condensed morphology consistent with chondrocytes. Over half of the PDGFRα- and SOX9-expressing cells were marked by the TDTOMATO fluorophore (Figure 4G). These results suggest that at the 1-week time point, *Hoxa11*-lineage cells begin to differentiate toward heterotopic bone.

Hoxa11-lineage cells differentiate into mature ectopic bone

Finally, to determine whether *Hoxa11*-lineage cells differentiate and contribute to the ectopic bone formation seen after injury, we analyzed IF labeling at weeks 3 and 9 as well as the snATAC and scRNA transcriptome data from MSCs that were derived from cells 6 weeks post injury (Figure 5).

IF labeling and imaging performed at the 3-week time point demonstrated that *Hoxa11*-lineage cells differentiated into an osteogenic/chondrogenic state. PDGFRα co-localized with TDTOMATO-expressing cells near the periphery of condensing HO anlagen (Figure 5A). SOX9 expression was paired with chondrocyte morphology of TDTOMATO-expressing cells within the HO anlagen (Figure 5A). Osteoblast markers RUNX2 and OPN co-localized with TDTOMATO expression within the HO anlagen as well at the 3-week time point (Figure 5A). Over 50% of the antigen-expressing cells were marked by the *Hoxa11*-lineage tracer at 3 weeks (Figure 5A).

Analysis of snATAC data showed that while the mean reads of open chromatin had decreased since the 1-week time point, chondrogenic and osteogenic gene loci remained partially open (Figure 5B).

Analysis of the scRNA transcriptome of the *TdTomato*-expressing clusters post injury demonstrated *TdTomato* expression in all five clusters at 6 weeks (Figures 5C and 5D). *Scx* and *Tnmd* were expressed in *Hoxa11*-lineage MSC:0 and Teno:16 at 6 weeks; however, chondrogenic and osteogenic differentiation gene expression was limited to MSC:0 (Figure 5E). While *Sox9* was expressed in MSC:2 at 6 weeks post injury, the expression level remained constant throughout the uninjured, 1-week post-injury, and 6-week post-injury samples (Figures 5E, 3D, and 4D). The osteogenic and chondrogenic genes that were upregulated in MSC:14 and Teno:16 at the 1-week post-injury time point resolved back to the uninjured baseline at 6 weeks post injury, while MSC:0 maintained osteogenic and chondrogenic expression (Figure 5E). These results suggest that MSC:0 has formed the heterotopic bone and remains chondrogenic and osteogenic.

IF labeling at the 9-week time point, when mature bone is present, showed *Hoxa11*-lineage *TdTomato*-expressing cells within fully formed ectopic bone. Near the periphery of the ectopic bone, *TdTomato*$^+$ cells were marked by RUNX2 (Figure 5F). OPN and SP7 marked *TdTomato*$^+$ cells and were entrapped within the mature HO (Figure 5F). Lastly, *TdTomato*$^+$ cells were co-localized with PLIN1, a lipid support protein within adipocytes, suggesting that *Hoxa11*-lineage cells can differentiate into adipocytes. This is also evidenced by snATAC results of adipogenic genes in MSC:0 cells (Figure S5). At the 9-week time point, over 60% of antigen-expressing cells were marked by the *Hoxa11* TDTOMATO lineage tracer (Figure 5G). These results confirmed that *Hoxa11*-lineage cells differentiated into ectopic bone following injury through a paired chondrogenic and osteogenic phenotype.

DISCUSSION

HO is a tightly orchestrated process regulated by various transcription factors. The expression of *Hox* genes and

Figure 4. *Hoxa11* marks a unique osteo/chondro/teno cell type following injury

(A) snATAC-seq of *TdTomato*-expressing cluster MSC:0 1 week post injury. Genes shown are important in chondrogenesis and osteogenesis. Bars represent mean value of reads.

(B) UMAP plot of cells 1 week following BT injury.

(C) UMAP feature plot depicting *TdTomato* expression (top left), violin plot showing *TdTomato* expression at 1 week following BT injury for reference (top right, from Figure 1C), and cell counts of all clusters (bottom).

(D) Violin plots of genes necessary in differentiation of tenocytes (left), chondrocytes (middle), and osteoblasts (right).

(E) Bar chart visualizing the number of *TdTomato*$^+$ cells in MSC cluster 0 expressing *Sox9*, *Runx2*, *Sox9* and *Runx2*, or neither.

(F) Confocal microscopy images of the hindlimb 1 week following BT injury with tile scan (n = 2 mice/antigen of interest, n = 3 images/mouse) (left). Dotted line shows the HO site while dashed line shows labeled calcaneus and tibia bones. The yellow box highlights region of 63× total zoom inset images (right). Sections were immunolabeled with PDGFRα, SOX9, and pSMAD3 (bottom). Blue chevrons mark *Hoxa11*iTom cells co-labeled with specified antibodies. Yellow scale bar, 500 μm; white scale bars, 50 μm.

(G) Bar chart showing mean with SEM of cell-count quantification of antigen-expressing cells co-labeled with TDTOMATO fluorophore.

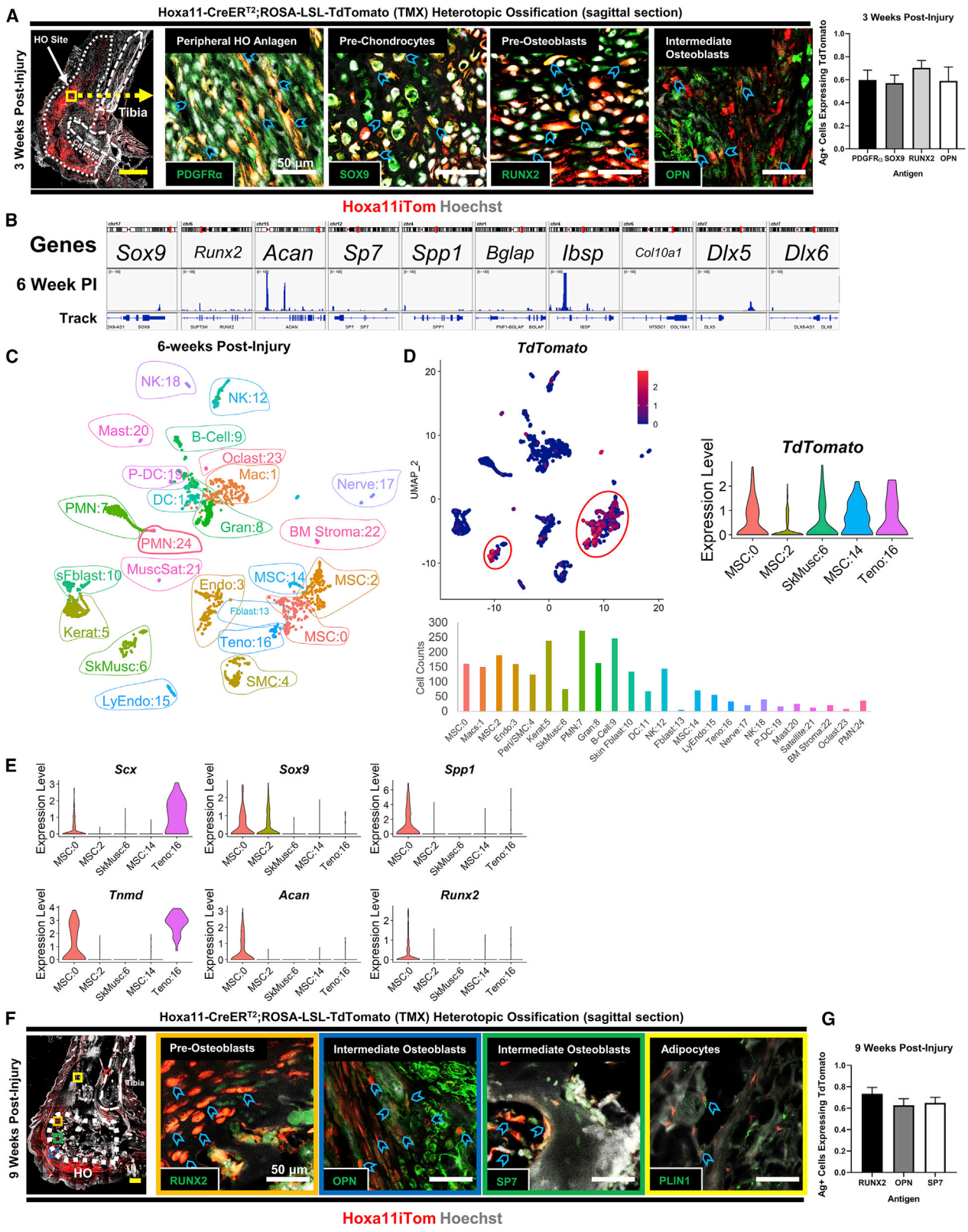

(legend on next page)

proteins help define regional formation of structures throughout development. However, recent studies have found that *Hox* genes may play a role that extends beyond embryonic patterning and formation of the musculoskeletal system in murine limbs, specifically within the limb zeugopod (Pineault et al., 2019; Rux et al., 2016; Swinehart et al., 2013). *Hoxa11*-lineage cells were found to be self-renewing and persistent throughout embryonic development and adulthood, serving a critical role in fracture repair (Pineault et al., 2019).

In the current study, we investigated whether cells that were previously described as self-renewing *Hoxa11*-lineage adult skeletal progenitor-enriched MSCs (Pineault et al., 2019) were involved in the aberrant cell fate and ectopic bone formation after traumatic injury. To analyze this, we used a *Hoxa11* lineage-tracing mouse line in conjunction with a mouse model of traumatic injury in the zeugopod. We found that in the uninjured limb, *Hoxa11*-lineage cells were located within tendon and muscle and were not primed to differentiate into cartilage or bone. *TdTomato* expression in muscle fibers is a novel finding; however, it is outside the scope of this work. Previous research has identified Hoxa11eGFP expression within tendon but not muscle fibers (Rux et al., 2016; Swinehart et al., 2013); however, they did not use the lineage-tracing model used in this study. Previous research has found that local MSCs differentiate into HO and contribute to wound healing (Agarwal et al., 2017b; Dey et al., 2016; Eming et al., 2014). These cells are already present and awaiting signals from the surrounding tissue to undergo proliferation and differentiation to repair the injured tissue, rather than stemming from circulation (Loder et al., 2018). After injury, we found upregulation of osteogenic and chondrogenic genes in the *Hoxa11*-lineage cells as well as increased levels of open chromatin in genes responsible for osteochondral MSC differentiation. After 9 weeks, osteoblasts were positive for the TDTOMATO reporter, demonstrating that *Hoxa11*-lineage cells were responsible for the ectopic bone formation after injury.

The use of scRNA transcriptome analysis of cells from *Hoxa11*-lineage reporter in the uninjured limb and 1 week and 6 weeks after injury allowed us to identify five clusters that expressed the *TdTomato* reporter gene. Furthermore, this system allowed us to track the differentiation of these cells after trauma. *Hoxa11*-lineage clusters were very heterogeneous, containing markers that have previously been reported to mark cells contributing to the formation of healed bone and ectopic bone. Four clusters—MSC:0, MSC:2, MSC:14, and Teno:16—expressed the mesenchymal markers *Pdgfra* and *Prrx1* (Agarwal et al., 2016a; Farahani and Xaymardan, 2015). Additionally, we found genes related to osteoblasts and osteocyte differentiation including *Cxcl12* (Ding and Morrison, 2013; clusters MSC:0, MSC:2, MSC:14, and Teno:16), *Clec11a* (Yue et al., 2016; clusters MSC:0, MSC:2, MSC:14, and MSC:16), *Clec3b* (Iba et al., 2001; clusters MSC:0, MSC:2, and MSC:14), and *En1* (Deckelbaum et al., 2012; clusters MSC:0 and MSC:14). Furthermore, we noted expression of *Pdpn* and *Cd164* in clusters MSC:0, MSC:2, MSC:14, and Teno:16 that have been described to mark multipotent human skeletal stem cells (Chan et al., 2018; Walmsley et al., 2015). Although characterization of bone progenitor cells has posed a challenge due to overlapping and conflicting findings (Ono et al., 2019), our results identified previously described marker gene expression found within the *Hoxa11*-lineage cells within our single-cell dataset. Leptin receptor, which is expressed by the gene *Lepr*, has been previously used to mark bone marrow mesenchymal stromal cells that regenerate bone following injury (Zhou et al., 2014) and was expressed in MSC:14. This is

Figure 5. *Hoxa11*-lineage cells differentiate into ectopic chondrocyte, osteoblasts, and adipocytes

(A) Confocal microscopy images of the hindlimb 3 weeks following BT injury, including tile scan image with dashed lines marking native bone and dotted line marking HO (left) and 63× insets of region of interest (n = 2 mice/antigen of interest, n = 3 images/mouse). Sections were immunolabeled with indicated antibodies (bottom). Blue chevrons mark *Hoxa11*iTom cells co-labeled with specified antibodies. Yellow scale bar, 500 μm; white scale bars, 50 μm. Right: bar chart showing mean with SEM of cell-count quantification of antigen-expressing cells co-labeled with TDTOMATO fluorophore.

(B) snATAC-seq of *TdTomato*-expressing cluster MSC:0 6 weeks post injury. Genes shown are important in chondrogenesis and osteogenesis. Bars represent mean value of reads.

(C) UMAP plot of cells 6 weeks following BT injury.

(D) UMAP feature plot depicting *TdTomato* expression with clusters expressing *TdTomato* circled in red (top left), violin plot showing *TdTomato* expression 6 weeks following BT injury for reference (top right, from Figure 1C), and cell counts across all clusters (bottom).

(E) Violin plots of genes necessary in differentiation of tenocytes (left), chondrocytes (middle), and osteoblasts (right).

(F) Confocal microscopy images of the hindlimb 9 weeks (bottom) following BT injury with tile scan for reference (n = 2 mice/antigen of interest, n = 3 images/mouse) (left). Dotted line shows the HO site while dashed line shows labeled tibia bone. Calcaneus not labeled at 9-week time point as it is surrounded by heterotopic bone. The colored boxes highlight regions of 63× total zoom inset images (right). Sections were immunolabeled with indicated antibodies. Blue chevrons mark *Hoxa11*iTom cells co-labeled with specified antibodies. Yellow scale bar, 500 μm; white scale bars, 50 μm.

(G) Bar chart showing mean with SEM of cell-count quantification of antigen-expressing cells co-labeled with TDTOMATO fluorophore.

particularly interesting, as these cells were previously known to reside within the bone marrow. As the cells that were sequenced by scRNA were harvested from the Achilles' tendon and surrounding soft tissue, purposefully excluding cells of the bone marrow, this would suggest that a population of *Lepr*$^{+}$ cells exists outside of the bone marrow prior to injury.

Previous studies have utilized various genetic models to study the cells that contribute to HO, yet these models have had significant limitations, including a lack of region specificity complicating interpretations regarding cell origin. Additionally, the many cell-specific reporters tend to mark terminally differentiated cell types but do not allow the characterization of the more primitive cells of interest. Cre mouse lines *Prrx1Cre*, *Nfatc1Cre*, *Glast1Cre*, *Gli1-Cre*, and *ScxCre*, while useful in marking specific HO progenitor cells that eventually form HO, do not mark the most primitive MSCs (Agarwal et al., 2016b, 2017b; Dey et al., 2016; Kan et al., 2013, 2018). Thus, there remains a need to develop a model that reliably marks and traces site-specific, multipotent lineage stem cells that form heterotopic bone. In this study, we characterized a novel inducible *Hoxa11* mouse line that marks zeugopod MSCs and traced these cells through ectopic bone formation. The *Hoxa11* cells expressed chrondrogenic marker SOX9 and early osteogenic markers RUNX2 and OPN shortly after BT injury. A later osteogenic marker, SP7, was observed after bony growth was observed. These findings suggest that the *Hoxa11-CreER*^{T2} mouse is an effective and reliable method to mark progenitor cells to evaluate the pathogenesis of HO restricted to MSCs in the zeugopod.

There are several benefits to the *Hoxa11-CreER*^{T2} model for studying HO formation. Performing experiments with the BT mouse model within the *Hoxa11-CreER*^{T2}*;ROSA26-LSL-TdTomato* mice allows for consistent and reliable visualization of cells that differentiate into HO by an endogenous fluorophore, which avoids the complications of IF staining. Furthermore, this mouse line also ensures that cells visualized, or modifications made with the Cre recombinase, are restricted to the zeugopod due to the isolated expression of the *Hoxa11* patterning gene.

This system is useful for evaluating other tissue-resident stem cells that give rise to mature tendon or adipose tissue. Lineage-traced *Hoxa11* cells were found in abundance in uninjured and injured Achilles' tendon. Current methods to evaluate the stem cells that differentiate into tendon are limited to *ScxCre*; however, these cells are classified as differentiated progenitors rather than the more primitive *Hoxa11*-expressing cells (Yoshimoto et al., 2017), which is consistent with trajectory analyses. We found an *Scx*$^{+}$ cluster that expressed *TdTomato* in the uninjured limb (Teno:16). Following injury, *TdTomato* and *Scx* expression were found in MSC:0 as well. Additionally, our study demonstrated the co-localization of TDTOMATO and perilipin, suggesting that *Hoxa11* cells likely can give rise to mature adipocytes, which was supported by snATAC findings. This model may also be useful in studying the differentiation of mesenchymal precursors to adipocytes, as *AdiponectinCre* and *PdgfraCre* models have both been utilized to study adipogenesis (Lee et al., 2012; Wang et al., 2010) and share similar disadvantages in systemic deletion of genes.

Lastly, the combined chondrogenic and osteogenic cell state provides additional insight into the process by which MSCs differentiate into ectopic bone following injury. These findings suggest that one *Hoxa11*-lineage cell type, described in this paper as MSC:0, begins in a stem state that, following injury, progresses toward a combined osteogenic and chondrogenic cell, highlighted by the expression of *Sox9*, *Acan*, *Runx2*, and *Spp1*. Expression of *Runx2* at the 1-week time point suggests for the first time that HO is formed by intramembranous ossification (Takarada et al., 2016), which is the ossification directly from preosteogenic conditions, as well as endochondral ossification, which requires a chondrogenic state before ossification.

In conclusion, we utilize the *Hoxa11-CreER*^{T2}*;ROSA-LSL-TdTomato* mouse to study the contribution of site-specific MSCs to HO. This validated and reliable model can be used to further study the MSCs responsible for HO, as well as studying stem/precursor cells that contribute to various extremity pathologies within fat, muscle, tendon, and bone. These techniques can be utilized to evaluate the efficacy of pharmacological and therapeutic interventions to limit HO formation.

EXPERIMENTAL PROCEDURES

Mouse model

All animal procedures were carried out in accordance with the guidelines provided in the Guide for the Use and Care of Laboratory Animals from the Institute for Laboratory Animal Research (ILAR, 2011), and conducted in compliance with State and Federal law and standards of the US Department of Health and Human Services, and were approved by the Institutional Animal Care and Use Committee of the University of Michigan (PRO0007930). All animals were housed in the University of Michigan's Unit for Laboratory Animal Medicine-supervised, Assessment and Accreditation of Laboratory Animal Care-accredited facilities at 18°C–22°C, on a 12:12-h light/dark cycle with *ad libitum* access to food and water. *Hoxa11-CreER*^{T2}*;ROSA-TdTomato* mice were provided generously by the Wellik Laboratory (University of Wisconsin, Madison, WI) and bred in-house (Pineault et al., 2019).

Additional experimental procedures

Methodology for the tamoxifen induction, BT surgery, scRNA-seq, snATAC-seq, bioinformatics, IF histology, confocal microscopy, and image analysis can be found in Supplemental information.

ACCESSION NUMBERS

scRNA-seq and snATAC-seq data can be accessed on the Gene Expression Omnibus at accession number GEO: GSE150995.

SUPPLEMENTAL INFORMATION

Supplemental Information can be found online at https://doi.org/10.1016/j.stemcr.2021.01.011.

AUTHOR CONTRIBUTIONS

C.A.P.: Authorship of manuscript, developed experimental design, performed and analyzed IF histology microscopy, performed and interpreted scRNA-seq and snATAC-seq results. A.K.H.: Contributed to manuscript, developed experimental design, executed mouse surgery, isolated and prepared scRNA-seq and snATAC-seq samples. C.H.: Performed IF histology and microscopy, contributed to experimental design. S.M.: Contributed to manuscript and performed bioinformatics analyses. K.P.: Performed snATAC analysis and contributed to manuscript. N.L.: Assisted in tissue sectioning, histology staining, confocal imaging, and image analysis. J.N.: Assisted in histology staining. Y.S.: Assisted in histology staining. Y.-H.C.: Performed Velocyto analysis. N.E.: Assisted in experimental design. N.V.: Performed tissue harvests and sectioning. P.Y.: Performed tissue harvests and sectioning. N.P.: Assisted in IF histology and microscopy. J.G.: Assisted in image quantification. H.R.: Assisted in image quantification. R.N.: Assisted in image quantification. K.K.: Bred and maintained mouse colony. K.V.: General support of laboratory techniques and laboratory management. A.L.S.: Contributed to manuscript. G.E.H.: Contributed to manuscript. J.Y.S.: Provided mouse breeding pairs and contributed to manuscript. D.M.W.: Provided mouse breeding pairs and contributed to manuscript. B.L.: Principal investigator of the laboratory. Developed experimental design and contributed to manuscript.

ACKNOWLEDGMENTS

The authors would like to acknowledge Dr. Stephen Weiss of the University of Michigan for providing insightful guidance on experimental design. Some figure elements were generated in BioRender.com.

B.L. is supported by funding from NIH/NIAMS; NIH1-R01AR071379, NIHR01GM123069, American College of Surgeons Clowes Award, and International FOP Association.

Received: June 19, 2020
Revised: January 19, 2021
Accepted: January 21, 2021
Published: February 18, 2021

REFERENCES

Agarwal, S., Loder, S., Brownley, C., Cholok, D., Mangiavini, L., Li, J., Breuler, C., Sung, H.H., Li, S., Ranganathan, K., et al. (2016a). Inhibition of Hif1alpha prevents both trauma-induced and genetic heterotopic ossification. Proc. Natl. Acad. Sci. U S A *113*, E338–E347.

Agarwal, S., Loder, S.J., Breuler, C., Li, J., Cholok, D., Brownley, C., Peterson, J., Hsieh, H.H., Drake, J., Ranganathan, K., et al. (2017a). Strategic targeting of multiple BMP receptors prevents trauma-induced heterotopic ossification. Mol. Ther. *25*, 1974–1987.

Agarwal, S., Loder, S.J., Cholok, D., Peterson, J., Li, J., Breuler, C., Cameron Brownley, R., Hsin Sung, H., Chung, M.T., Kamiya, N., et al. (2017b). Scleraxis-lineage cells contribute to ectopic bone formation in muscle and tendon. Stem Cells *35*, 705–710.

Agarwal, S., Loder, S.J., Sorkin, M., Li, S., Shrestha, S., Zhao, B., Mishina, Y., James, A.W., and Levi, B. (2016b). Analysis of bone-cartilage-stromal progenitor populations in trauma induced and genetic models of heterotopic ossification. Stem Cells *34*, 1692–1701.

Bergen, V., Lange, M., Peidli, S., Wolf, F.A., and Theis, F.J. (2020). Generalizing RNA velocity to transient cell states through dynamical modeling. Nat. Biotechnol. *38*, 1408–1414.

Chan, C.K.F., Gulati, G.S., Sinha, R., Tompkins, J.V., Lopez, M., Carter, A.C., Ransom, R.C., Reinisch, A., Wearda, T., Murphy, M., et al. (2018). Identification of the human skeletal stem cell. Cell *175*, 43–56 e21.

Chereji, R.V., Eriksson, P.R., Ocampo, J., Prajapati, H.K., and Clark, D.J. (2019). Accessibility of promoter DNA is not the primary determinant of chromatin-mediated gene regulation. Genome Res. *29*, 1985–1995.

Comazzetto, S., Murphy, M.M., Berto, S., Jeffery, E., Zhao, Z., and Morrison, S.J. (2019). Restricted hematopoietic progenitors and erythropoiesis require SCF from leptin receptor+ niche cells in the bone marrow. Cell Stem Cell *24*, 477–486 e476.

Deckelbaum, R.A., Holmes, G., Zhao, Z., Tong, C., Basilico, C., and Loomis, C.A. (2012). Regulation of cranial morphogenesis and cell fate at the neural crest-mesoderm boundary by engrailed 1. Development *139*, 1346–1358.

Dey, D., Bagarova, J., Hatsell, S.J., Armstrong, K.A., Huang, L., Ermann, J., Vonner, A.J., Shen, Y., Mohedas, A.H., Lee, A., et al. (2016). Two tissue-resident progenitor lineages drive distinct phenotypes of heterotopic ossification. Sci. Transl. Med. *8*, 366ra163.

Ding, L., and Morrison, S.J. (2013). Haematopoietic stem cells and early lymphoid progenitors occupy distinct bone marrow niches. Nature *495*, 231–235.

Eming, S.A., Martin, P., and Tomic-Canic, M. (2014). Wound repair and regeneration: mechanisms, signaling, and translation. Sci. Transl. Med. *6*, 265sr266.

Farahani, R.M., and Xaymardan, M. (2015). Platelet-derived growth factor receptor alpha as a marker of mesenchymal stem cells in development and stem cell biology. Stem Cells Int. *2015*, 362753.

Foley, K.L., Hebela, N., Keenan, M.A., and Pignolo, R.J. (2018). Histopathology of periarticular non-hereditary heterotopic ossification. Bone *109*, 65–70.

Genet, F., Kulina, I., Vaquette, C., Torossian, F., Millard, S., Pettit, A.R., Sims, N.A., Anginot, A., Guerton, B., Winkler, I.G., et al. (2015). Neurological heterotopic ossification following spinal cord injury is triggered by macrophage-mediated inflammation in muscle. J. Pathol. *236*, 229–240.

Gulati, G.S., Sikandar, S.S., Wesche, D.J., Manjunath, A., Bharadwaj, A., Berger, M.J., Ilagan, F., Kuo, A.H., Hsieh, R.W., Cai, S.,

et al. (2020). Single-cell transcriptional diversity is a hallmark of developmental potential. Science *367*, 405–411.

Hsieh, H.H.S., Agarwal, S., Cholok, D.J., Loder, S.J., Kaneko, K., Huber, A., Chung, M.T., Ranganathan, K., Habbouche, J., Li, J., et al. (2019). Coordinating tissue regeneration through transforming growth factor-beta activated kinase 1 inactivation and reactivation. Stem Cells *37*, 766–778.

Hwang, C., Marini, S., Huber, A.K., Stepien, D.M., Sorkin, M., Loder, S., Pagani, C.A., Li, J., Visser, N.D., Vasquez, K., et al. (2019). Mesenchymal VEGFA induces aberrant differentiation in heterotopic ossification. Bone Res. *7*, 36.

Iba, K., Durkin, M.E., Johnsen, L., Hunziker, E., Damgaard-Pedersen, K., Zhang, H., Engvall, E., Albrechtsen, R., and Wewer, U.M. (2001). Mice with a targeted deletion of the tetranectin gene exhibit a spinal deformity. Mol. Cell. Biol. *21*, 7817–7825.

Kan, C., Chen, L., Hu, Y., Ding, N., Li, Y., McGuire, T.L., Lu, H., Kessler, J.A., and Kan, L. (2018). Gli1-labeled adult mesenchymal stem/progenitor cells and hedgehog signaling contribute to endochondral heterotopic ossification. Bone *109*, 71–79.

Kan, L., Peng, C.Y., McGuire, T.L., and Kessler, J.A. (2013). Glast-expressing progenitor cells contribute to heterotopic ossification. Bone *53*, 194–203.

Komori, T. (2006). Regulation of osteoblast differentiation by transcription factors. J. Cell. Biochem. *99*, 1233–1239.

Komori, T. (2010). Regulation of bone development and extracellular matrix protein genes by RUNX2. Cell Tissue Res. *339*, 189–195.

Komori, T. (2017). Roles of runx2 in skeletal development. Adv. Exp. Med. Biol. *962*, 83–93.

La Manno, G., Soldatov, R., Zeisel, A., Braun, E., Hochgerner, H., Petukhov, V., Lidschreiber, K., Kastriti, M.E., Lonnerberg, P., Furlan, A., et al. (2018). RNA velocity of single cells. Nature *560*, 494–498.

Lee, Y.H., Petkova, A.P., Mottillo, E.P., and Granneman, J.G. (2012). In vivo identification of bipotential adipocyte progenitors recruited by beta3-adrenoceptor activation and high-fat feeding. Cell Metab. *15*, 480–491.

Li, R., Bernau, K., Sandbo, N., Gu, J., Preissl, S., and Sun, X. (2018). Pdgfra marks a cellular lineage with distinct contributions to myofibroblasts in lung maturation and injury response. eLife *7*, e36865.

Loder, S.J., Agarwal, S., Chung, M.T., Cholok, D., Hwang, C., Visser, N., Vasquez, K., Sorkin, M., Habbouche, J., Sung, H.H., et al. (2018). Characterizing the circulating cell populations in traumatic heterotopic ossification. Am. J. Pathol. *188*, 2464–2473.

Logan, M., Martin, J.F., Nagy, A., Lobe, C., Olson, E.N., and Tabin, C.J. (2002). Expression of Cre Recombinase in the developing mouse limb bud driven by a Prxl enhancer. Genesis *33*, 77–80.

Matsushita, Y., Nagata, M., Kozloff, K.M., Welch, J.D., Mizuhashi, K., Tokavanich, N., Hallett, S.A., Link, D.C., Nagasawa, T., Ono, W., et al. (2020). A Wnt-mediated transformation of the bone marrow stromal cell identity orchestrates skeletal regeneration. Nat. Commun. *11*, 332.

Miwa, H., and Era, T. (2018). Tracing the destiny of mesenchymal stem cells from embryo to adult bone marrow and white adipose tissue via PDGFRalpha expression. Development *145*, dev155879.

O'Rourke, M., Cullen, C.L., Auderset, L., Pitman, K.A., Achatz, D., Gasperini, R., and Young, K.M. (2016). Evaluating tissue-specific recombination in a PDGFRalpha-CreERT2 transgenic mouse line. PLoS one *11*, e0162858.

Ono, N., Balani, D.H., and Kronenberg, H.M. (2019). Stem and progenitor cells in skeletal development. Curr. Top. Dev. Biol. *133*, 1–24.

Pineault, K.M., Song, J.Y., Kozloff, K.M., Lucas, D., and Wellik, D.M. (2019a). Hox11 expressing regional skeletal stem cells are progenitors for osteoblasts, chondrocytes and adipocytes throughout life. Nat. Commun. *10*, 3168.

Qian, C., Wong, C.W.Y., Wu, Z., He, Q., Xia, H., Tam, P.K.H., Wong, K.K.Y., and Lui, V.C.H. (2017). Stage specific requirement of platelet-derived growth factor receptor-alpha in embryonic development. PLoS one *12*, e0184473.

Robledo, R.F., Rajan, L., Li, X., and Lufkin, T. (2002). The Dlx5 and Dlx6 homeobox genes are essential for craniofacial, axial, and appendicular skeletal development. Genes Dev. *16*, 1089–1101.

Rux, D.R., Song, J.Y., Swinehart, I.T., Pineault, K.M., Schlientz, A.J., Trulik, K.G., Goldstein, S.A., Kozloff, K.M., Lucas, D., and Wellik, D.M. (2016). Regionally restricted hox function in adult bone marrow multipotent mesenchymal stem/stromal cells. Dev. Cell *39*, 653–666.

Shahnazari, M., Chu, V., Wronski, T.J., Nissenson, R.A., and Halloran, B.P. (2013). CXCL12/CXCR4 signaling in the osteoblast regulates the mesenchymal stem cell and osteoclast lineage populations. FASEB J. *27*, 3505–3513.

Shi, Y., He, G., Lee, W.C., McKenzie, J.A., Silva, M.J., and Long, F. (2017). Gli1 identifies osteogenic progenitors for bone formation and fracture repair. Nat. Commun. *8*, 2043.

Shukunami, C., Takimoto, A., Nishizaki, Y., Yoshimoto, Y., Tanaka, S., Miura, S., Watanabe, H., Sakuma, T., Yamamoto, T., Kondoh, G., et al. (2018). Scleraxis is a transcriptional activator that regulates the expression of Tenomodulin, a marker of mature tenocytes and ligamentocytes. Sci. Rep. *8*, 3155.

Sorkin, M., Huber, A.K., Hwang, C., Carson, W.F.t., Menon, R., Li, J., Vasquez, K., Pagani, C., Patel, N., Li, S., et al. (2020). Regulation of heterotopic ossification by monocytes in a mouse model of aberrant wound healing. Nat. Commun. *11*, 722.

Sugimoto, Y., Takimoto, A., Akiyama, H., Kist, R., Scherer, G., Nakamura, T., Hiraki, Y., and Shukunami, C. (2013a). Scx+/Sox9+ progenitors contribute to the establishment of the junction between cartilage and tendon/ligament. Development *140*, 2280–2288.

Sugimoto, Y., Takimoto, A., Hiraki, Y., and Shukunami, C. (2013b). Generation and characterization of ScxCre transgenic mice. Genesis *51*, 275–283.

Swinehart, I.T., Schlientz, A.J., Quintanilla, C.A., Mortlock, D.P., and Wellik, D.M. (2013). Hox11 genes are required for regional patterning and integration of muscle, tendon and bone. Development *140*, 4574–4582.

Takarada, T., Nakazato, R., Tsuchikane, A., Fujikawa, K., Iezaki, T., Yoneda, Y., and Hinoi, E. (2016). Genetic analysis of Runx2 function during intramembranous ossification. Development *143*, 211–218.

Tirosh, I., Izar, B., Prakadan, S.M., Wadsworth, M.H., 2nd, Treacy, D., Trombetta, J.J., Rotem, A., Rodman, C., Lian, C., Murphy, G., et al. (2016). Dissecting the multicellular ecosystem of metastatic melanoma by single-cell RNA-seq. Science *352*, 189–196.

Torossian, F., Guerton, B., Anginot, A., Alexander, K.A., Desterke, C., Soave, S., Tseng, H.W., Arouche, N., Boutin, L., Kulina, I., et al. (2017). Macrophage-derived oncostatin M contributes to human and mouse neurogenic heterotopic ossifications. JCI Insight *2*, e96034.

Walmsley, G.G., Atashroo, D.A., Maan, Z.N., Hu, M.S., Zielins, E.R., Tsai, J.M., Duscher, D., Paik, K., Tevlin, R., Marecic, O., et al. (2015). High-throughput screening of surface marker expression on undifferentiated and differentiated human adipose-derived stromal cells. Tissue Eng. Part A *21*, 2281–2291.

Wang, X., Li, F., Xie, L., Crane, J., Zhen, G., Mishina, Y., Deng, R., Gao, B., Chen, H., Liu, S., et al. (2018). Inhibition of overactive TGF-beta attenuates progression of heterotopic ossification in mice. Nat. Commun. *9*, 551.

Wang, Z.V., Deng, Y., Wang, Q.A., Sun, K., and Scherer, P.E. (2010). Identification and characterization of a promoter cassette conferring adipocyte-specific gene expression. Endocrinology *151*, 2933–2939.

Yoshimoto, Y., Takimoto, A., Watanabe, H., Hiraki, Y., Kondoh, G., and Shukunami, C. (2017). Scleraxis is required for maturation of tissue domains for proper integration of the musculoskeletal system. Sci. Rep. *7*, 45010.

Yue, R., Shen, B., and Morrison, S.J. (2016). Clec11a/osteolectin is an osteogenic growth factor that promotes the maintenance of the adult skeleton. Elife *5*, e18782.

Zhao, H., Feng, J., Ho, T.V., Grimes, W., Urata, M., and Chai, Y. (2015). The suture provides a niche for mesenchymal stem cells of craniofacial bones. Nat. Cell Biol. *17*, 386–396.

Zhou, B.O., Yue, R., Murphy, M.M., Peyer, J.G., and Morrison, S.J. (2014). Leptin-receptor-expressing mesenchymal stromal cells represent the main source of bone formed by adult bone marrow. Cell Stem Cell *15*, 154–168.

Stem Cell Reports, Volume *16*

Supplemental Information

Novel Lineage-Tracing System to Identify Site-Specific Ectopic Bone Precursor Cells

Chase A. Pagani, Amanda K. Huber, Charles Hwang, Simone Marini, Karthik Padmanabhan, Nicholas Livingston, Johanna Nunez, Yuxiao Sun, Nicole Edwards, Yu-Hao Cheng, Noelle Visser, Pauline Yu, Nicole Patel, Joseph A. Greenstein, Husain Rasheed, Reagan Nelson, Karen Kessel, Kaetlin Vasquez, Amy L. Strong, Geoffrey E. Hespe, Jane Y. Song, Deneen M. Wellik, and Benjamin Levi

Figure S1

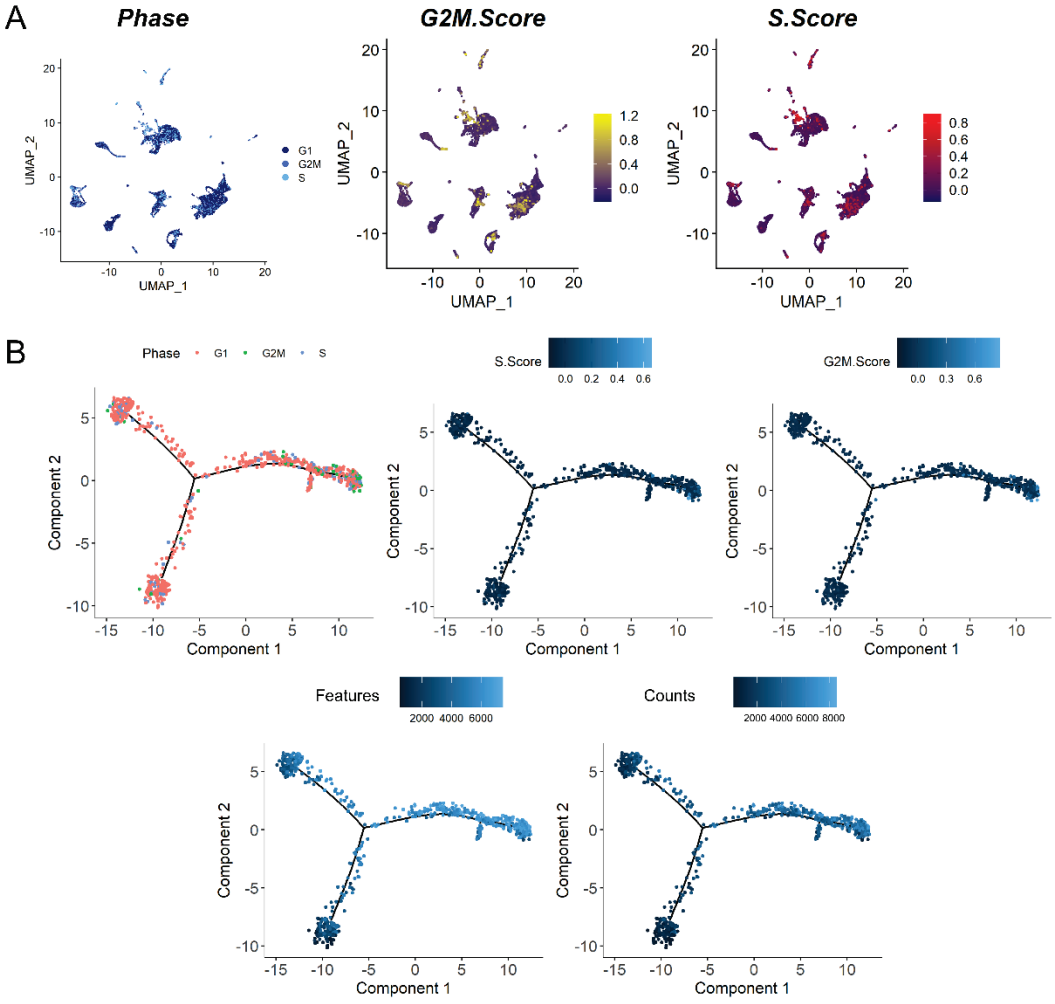

Figure S1. Single-Cell RNA sequencing cell cycle phase visualized on A) UMAP plots and B) trajectory analyses (top). Feature and counts also visualized on trajectories (bottom).

Figure S2

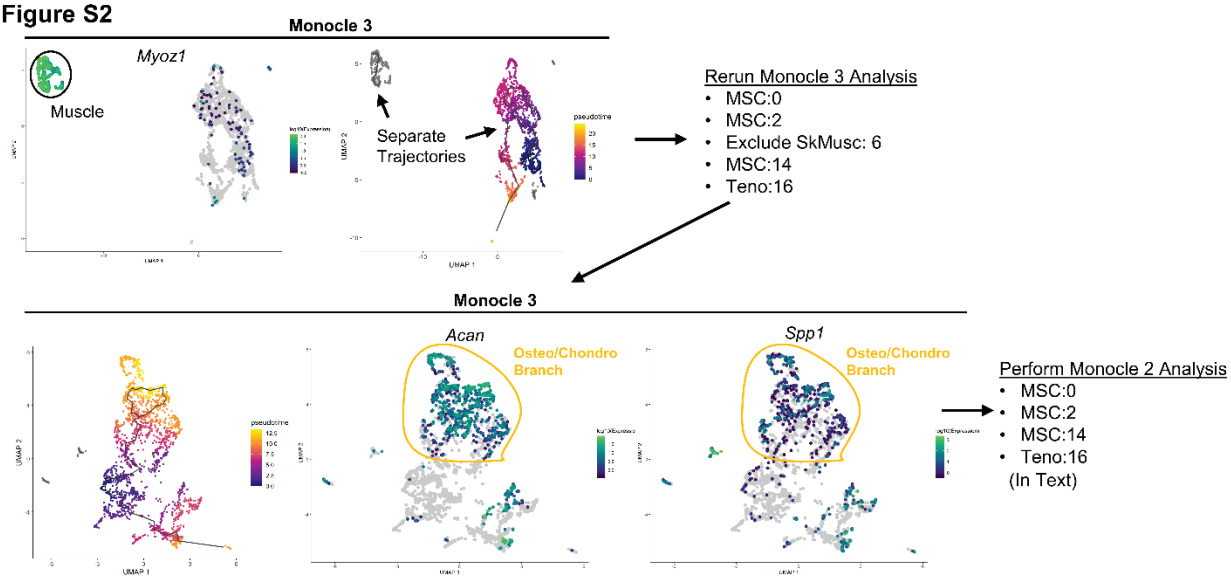

Figure S2. Single-Cell RNA-Sequencing Monocle 3 trajectory analysis. SkMusc:6 cluster did not share the same trajectory as other MSC populations. Monocle 3 was reperformed without SkMusc:6 to verify Osteo/Chondro branch was created by both Monocle 2 and 3.

Figure S3

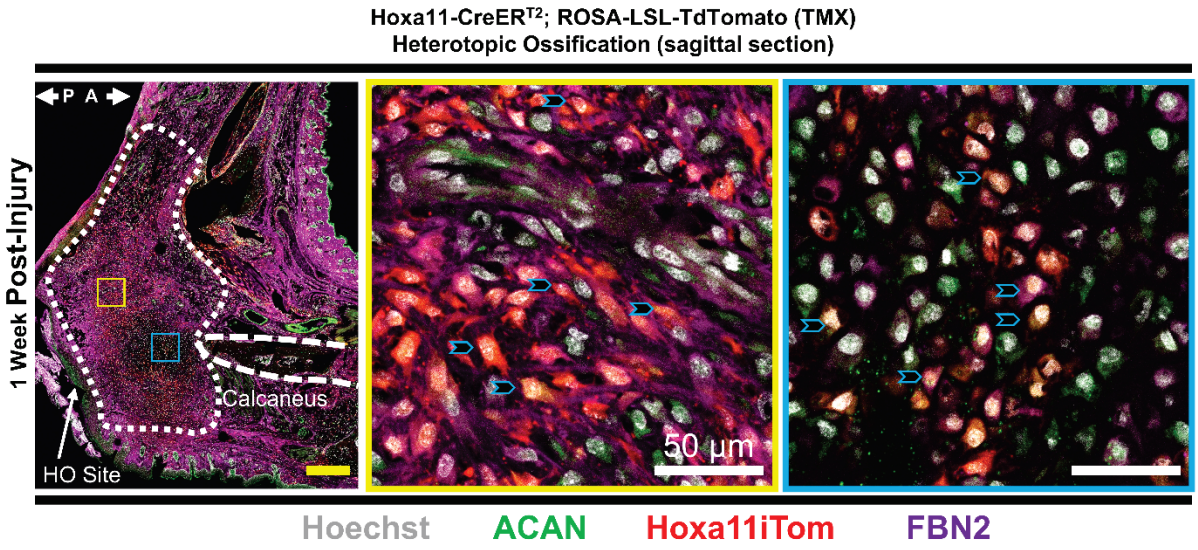

Figure S3. Confocal microscopy images of the hindlimb one-week following BT injury including tile scan image with dashed line marking calcaneus and dotted line marking HO (left) and 63x insets of region of interest. Sections were immunolabeled with indicated antibodies (bottom). Blue chevrons mark Hoxa11iTom cells co-labeled with specified antibodies. Yellow scale bars are 500 µm and white scale bars are 50 µm.

Figure S4

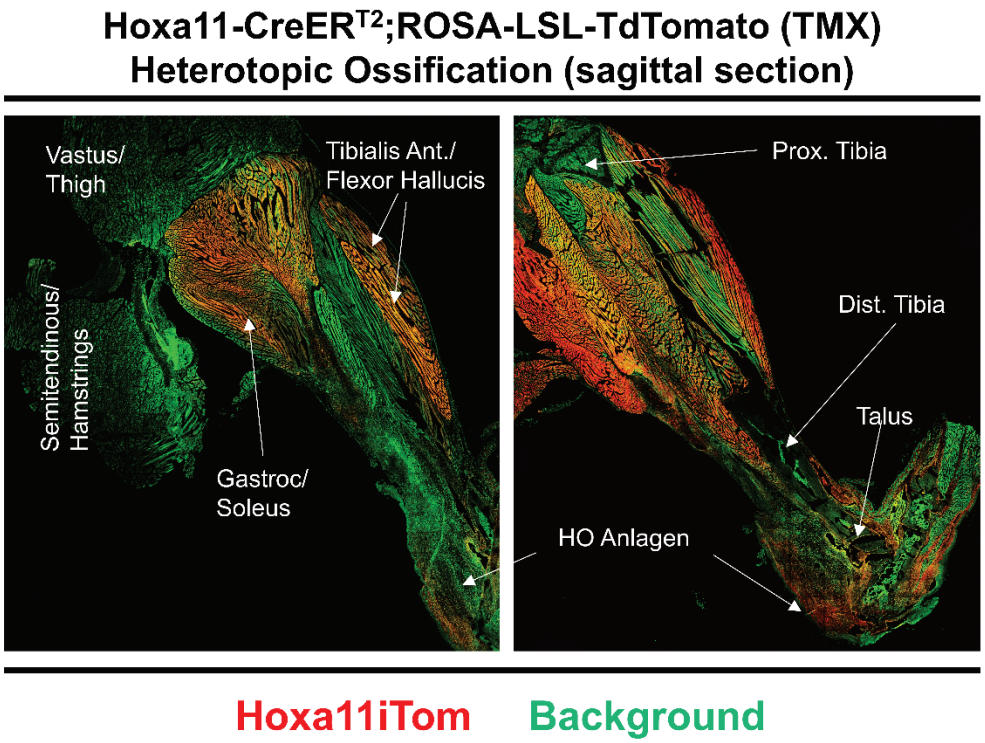

Figure S4. Confocal microscopy imaging shows that Hoxa11 TdTomato expression is limited to the limb zeugopod following burn/tenotomy injury and is not expressed in the upper mouse leg in two mouse samples (left and right). Background fluorescence (green), is shown for reference.

Figure S5

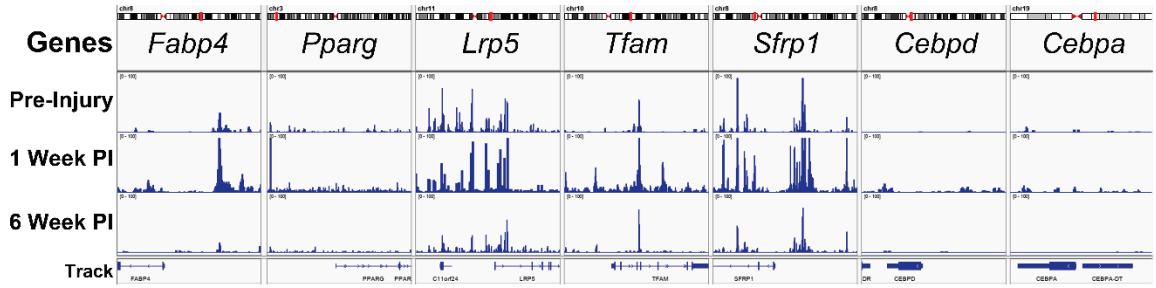

Figure S5. Single-nucleus ATAC sequencing of Hoxa11-lineage MSC cluster 0 shows open chromatin regions of adipogenic genes. Peaks show mean open chromatin reads.

Supplemental Table 1: Cluster marker genes.

Cluster	Gene Markers
MSC: 0	*Pdgfra*[1], *Acan*[2], *Fbn2*[3]
Macs: 1	*Mrc1*[4], *Csf1r*[5], *Adgre1*[6]
MSC: 2	*Pdgfra*[1], *Scara5*[7], *Clec3b*[8]
Endo: 3	*Pecam1*[9], *Mcam*[10]
Peri/SMC: 4	*Pdgfrb*[11], *Myh11*[12], *Abcc9*[13], *Pln*[14]
Kerat: 5	*Dmkn*[15], *Krt1*[16]
SkMusc: 6	*Des*[17], *Myoz1*[18]
PMN: 7	*Cxcr2*[19], *Camp*[20], *Mmp9*[21]
Gran: 8	*Ccr2*[22], *Il1b*[23]
B-Cell: 9	*Igkc*[24]
Skin Fblast: 10	*Krt15*[25], *Dmkn*[15]
DC: 11	*H2-Ab1*[26], *Il1b*[27], *Ccr2*[28]
NK: 12	*Il2rb*[29], *Cd2*[30]
Fblast: 13	*Col3a1*[31], *Sparc*[32], *Col1a1*[33], *Bgn*[34]
MSC: 14	*Pdgfra*[1], *Twist1*[35], *Pth1r*[36], *Wnt5a*[37]
LyEndo: 15	*Prox1*[38], *Flt4*[39]
Teno: 16	*Tnmd*[40], *Scx*[41], *Comp*[42]
Nerve: 17	*Sox10*[43], *Kcna1*[44], *Plp1*[45]
NK: 18	*Il2rb*[29], *Cd2*[30], *Cd7*[46]
P-DC: 19	*Cd7*[47], *Siglec*[48]
Mast: 20	*Cpa3*[49]
Satellite: 21	*Pax7*[50]
Stroma: 22	*Itgb4*[51], *Lepr*[52]
Oclast: 23	*Ocstamp*[53], *Mmp9*[54]
PMN: 24	*Fcnb*[55]

1. (Morikawa et al., 2009)
2. (Ono et al., 2014)
3. (Davis et al., 2014)
4. (Gordon and Martinez, 2010)
5. (Sherr et al., 1985)
6. (Waddell et al., 2018)
7. (Lee et al., 2017)
8. (Noack et al., 2014)
9. (Park et al., 2015)
10. (Wragg et al., 2016)
11. (Hou et al., 2018)
12. (Ray et al., 2020)
13. (Bondjers et al., 2006)
14. (Vanlandewijck et al., 2018)
15. (Matsui et al., 2004)
16. (Tao et al., 2007)
17. (Paulin and Li, 2004)
18. (Roberts et al., 2018)
19. (Sun et al., 2019)
20. (Herster et al., 2020)
21. (Wang et al., 2019b)
22. (Nywening et al., 2018)
23. (Drummond et al., 2019)
24. (Schmidt et al., 2012)
25. (Liu et al., 2003)
26. (Tesone et al., 2016)
27. (Mitsialis et al., 2020)
28. (Ruhland et al., 2020)
29. (Fernandez et al., 2019)
30. (Liu et al., 2016)
31. (Wang et al., 2019a)
32. (Drev et al., 2019)
33. (Li et al., 2020)
34. (Zhou et al., 2020)
35. (Fan et al., 2020)
36. (Cui et al., 2020)
37. (Diederichs et al., 2019)
38. (Wigle and Oliver, 1999)
39. (Karkkainen et al., 2004)
40. (Docheva et al., 2005)
41. (Huang et al., 2019)
42. (Smith et al., 1997)
43. (Fujiwara et al., 2014)
44. (Arroyo et al., 2001)
45. (Shy et al., 2003)
46. (Rabinowich et al., 1994)
47. (Zalmai et al., 2020)
48. (Perez-Zsolt et al., 2019)
49. (Lilla et al., 2011)
50. (Sambasivan et al., 2011)
51. (Bierie et al., 2017)
52. (Zhou et al., 2014)
53. (Yang et al., 2008)
54. (Sundaram et al., 2007)
55. (Tian et al., 2020)

Supplemental Table 2: Antibodies and dilutions used for immunofluorescent histology.

Antibody	Supplier and Catalogue #	Dilution (IF)
PDGFRα (goat)	R&D: AF1062	1:25
SOX9 (rabbit)	Abcam: ab185230	1:50
Phosphorylated SMAD3 (rabbit)	Novus: NBP1-77836	1:50
RUNX2 (rabbit)	Abcam: ab23981	1:50
Osteopontin (goat)	R&D: AF808	1:50
Osterix (rabbit)	Abcam: ab22552	1:50
Perilipin-1 (rabbit)	Cell Signaling: #9349	1:50
FBN2 (mouse)	Santa Cruz: sc-393968	1:50
ACAN (rabbit)	Abcam: ab36831	1:50
Alexa Fluor 488 (anti-goat)	Invitrogen: a21202	1:200
Alexa Fluor 647 (anti-goat)	Invitrogen: a21447	1:200
Alexa Fluor 647 (anti-rabbit)	Invitrogen: a31573	1:200
Hoechst 33342	Thermofisher: H3570	1:2000

SUPPLEMENTAL EXPERIMENTAL PROCEDURES

Tamoxifen Induction

Hoxa11-CreERT2;ROSA-TdTomato male and female mice six weeks of age were induced by feeding tamoxifen citrate chow (400mg/kg) for one week. Additionally, two intraperitoneal injections of tamoxifen (TMX; 75mg/kg) on days 0 and 2 were administered. Mice were allowed a washout period of four days before the BT injury.

BT Mouse Model

Mice were subjected to a BT injury as described previously [(Hwang et al., 2019); (Loder et al., 2018); (Sorkin et al., 2020)]. Briefly, mice were anesthetized and given buprenorphine analgesic prior to a complete transection of the left Achilles' tendon along with a dorsum burn of 30% total body surface area. The uninjured right leg served as an internal control.

Single Cell RNA Sequencing Preparation

scRNA and snATAC sequencing data are publicly available on GEO, GSE150995. Uninjured and post-surgery day 7 and 42 harvested tissue samples were processed as previously performed (Sorkin et al., 2020). Specifically, four mice were induced with tamoxifen as described in "Tamoxifen Induction" portion of experimental procedures. One mouse, serving as the uninjured control did not undergo the burn/tenotomy surgery. Three other mice underwent the burn/tenotomy injury. Cells from the uninjured control and from one of the injured mice were harvested seven days post-injury. Cells from the two remaining mice were harvested 42 days post-injury to ensure enough cells were harvested at the day 42 timepoint, as the inflammation and MSC proliferation at the injury site decreases significantly by day 42. Tissue was digested for 45 minutes in 750U/ml Type 1 Collagenase and 7U/ml Dispase II (Gibco) in Roswell Park Memorial Institute (RPMI) medium at 37°C under constant agitation at 180 rpm. Digestions were subsequently quenched with 2% FBS in PBS and filtered through 40µm sterile strainers. Cells were then washed in 2% FBS in PBS, counted and resuspended at a concentration of 1000-1200 cells/ul. Cell viability was assessed with Trypan blue exclusion on a Countess II (Thermo Fisher Scientific) automated counter and only samples with >85% viability were processed for further sequencing. For scRNA-seq we considered one replicate for day 0, one for day 7, and two replicates for day 42 and for snATAC-seq we considered one replicate each day 0, day 7, and day 42. Volumes corresponding to 5000 cell equivalents for scRNA-sequencing and 100,000 cell equivalents for snATAC-sequencing was removed for further processing. 5000 cells were processed for RNA libraries as described below. Before 10X library preparation, for snATAC-sequencing samples nuclei were extracted from 100,000 cells following the Nuclei Isolation for Single Cell ATAC Sequencing protocol (https://support.10xgenomics.com/single-cell-atac/sample-prep/doc/demonstrated-protocol-nuclei-isolation-for-single-cell-atac-sequencing) according to the manufacturer's guidelines. Library generation was performed using the 10x Genomics Chromium GEM Single Cell 3' Reagents kit v3.1 following the manufacturers protocol. Sequencing was performed on the Novaseq 6000 (Illumina, San Diego, CA, USA) S4 flowcell 300 cycle kit. This was loaded in order to target 500M reads/sample (5000 cells, 100K reads/cell), at 300pM (these were shared flowcells). The read length configuration was 150 x 8 x 150 cycles for Read 1, Index and Read 2, respectively. Cell Ranger Single Cell Software Suite 1.3 was used to perform sample de-multiplexing, barcode processing, and single cell gene counting (Alignment, Barcoding and UMI Count) at the University of Michigan Biomedical Core Facilities DNA Sequencing Core. For single ATAC sequencing, libraries were generated using the 10X Chromium Next GEM Single Cell ATAC kit v1.1; Chemistry with NextGEM Chip H. The sequencing was performed on the NovaSeq 6000 using the SP flowcell 100 cycle kit. Read lengths: 50 x 8 x 16 x 49.

Bioinformatics Analysis of Single Cell Sequencing Data

Seurat 3.1.1 (Butler et al., 2018) was used for downstream analysis. Cells with total expressed genes in the range of [500, 5000], [500, 6000], or [500, 7500], depending on the replicate, were retained. Cells with a fraction of mitochondrial gene UMIs higher than 0.25 were discarded. Filtered replicates were processed as Seurat objects. Seurat's FindVariableFeatures function was used with default parameters to determine highly variable genes, considering 2000 genes. Replicates were integrated according to the standard Seurat 3 workflow. Counts were normalized and variable genes were calculated (vst method) on each single replicate. The first 50 dimensions were considered for both finding integration anchors and integrate the replicates. The integrated set was then scaled, regressing out cell cycle gene scores and fraction of the mitochondrial gene UMIs. Unsupervised clustering was applied to the integrated set to find the cell communities (Louvain algorithm, resolution 0.35), leading to 25 clusters. The code to generate the Seurat object is available at https://github.com/smarini/Single-Cell-Downstream-analysis-Pagani-et-al.-2020. Markers for each cluster were calculated with FindMarkers using the negative binomial generalized linear model and ranked according to the difference in the fractions of cells expressing each marker

within cluster versus the rest of the considered cells. Clusters were labeled as cell type according to characteristic genes. After this, gene expression from all clusters were used to align the snATAC sequencing data using Signac 3.1.5 (https://github.com/timoast/signac). Briefly, snATAC data from the three conditions - day 0, day 7, and day 42 were merged after limiting the dataset to those cells that have at least 100 features. The resulting combined Seurat object was then normalized using default parameters and top variable features (peak accessibility) using a minimum cutoff of 20 cells were calculated. Dimension reduction was done using UMAP using dimensions 2 through 30 as input features. Unique clusters were determined using a shared nearest neighbor modularity optimization-based clustering algorithm with a resolution of 0.4. scRNA-seq data was used to guide the cluster labeling using `cca` reduction using the FindTransferAnchors function. This resulted in 9 cell-type based clusters in the snATAC data. Cells present in cluster 0 were extracted and bigWig files were generated for each condition (day 0, day 7 and day 42) using sinto (https://timoast.github.io/sinto/basic_usage.html#create-scatac-seq-fragments-file) and deeptools (Ramirez et al., 2016). Cells that had a least one count of *TdTomato* fluorophore transcript were included to create Figure 4E. Cells were characterized as *Sox9*, *Runx2,* or *Sox9 and Runx2* if they had at least one count of the respective gene transcript.

Cell Trajectories

Clusters 0, 2, 14, and 16 were used for cell trajectory analysis. Only cells with at least one count of *TdTomato* fluorophore transcript were included in the analysis. Cell trajectories were calculated with Monocle 2.13.0 (Trapnell et al., 2014), based on the top 2000 overall variable genes, ranked by scaled dispersion, obtained from Seurat. Further analysis using Monocle 3 0.2.3.0 confirmed that SkMusc:6 cluster formed a separate trajectory (Cao et al., 2019). The first 100 dimensions were considered. CytoTrace analysis were performed on the same cells through the internet application "Run Cytotrace" (https://cytotrace.stanford.edu/). The aligned bam files were subjected to Velocyto pipeline to obtain the counts of unspliced and spliced reads (La Manno et al., 2018). Cluster, cell features, and embedding information were extracted from the Seurat object in R and output to Python to integrate with the count matrix. The matrix was subsequently piped into the scVelo for RNA velocity estimation ((Bergen et al., 2020)). Genes were filtered by setting a minimal count threshold as 20 and a minimal unspliced count threshold as 10, and selected the top 2000 genes. The matrix was normalized and log-transformed. The first and second order moments for each cell were computed based on the top 30 principal components and the nearest 200 neighbors. RNA velocity was estimated by using the dynamical model and constructed the stream velocity graph. The latent time of each cell was calculated using the tl.latent_time function. The stream plot and latent time scatter plot were shown with cells embedded on top of the previously computed UMAP coordinates.

Immunofluorescence Histology and Confocal Microscopy

Mouse hind limb samples were harvested at one, three, and nine weeks after BT injury. The uninjured right leg served as an internal control and was harvested one week following left leg injury. Legs were fixed in 4% paraformaldehyde for 24 hours, washed with phosphate-buffered saline (PBS, Gibco, Waltham, MA), and then decalcified for 5 weeks in 17% EDTA (Sigma Aldrich, St. Louis, MO). Tissues were flash frozen in optimal cutting media for sectioning. Samples were oriented in blocks for sagittal sectioning. Tissue was cut into 7 µm sections and stored at -80°C. Sections were thawed, washed in 1X tris-buffered saline with tween-20 (TBST: 90% H_2O, 10% 10x tris-buffered saline (Bio-Rad, Hercules, CA), 0.05% tween-20, Sigma Aldrich, St. Louis, MO)) in preparation for immunofluorescence staining. Sections were blocked with donkey-serum block (10 ml solution: 0.1g BSA powder, 0.2 ml serum, 0.1 ml 10% cold water fish skin gelatin, 0.05 ml 20% TritonX-100, 0.05 ml 10% Tween-20, 3.0 ml 1M glycine, 1.0 ml 10x TBS pH 8.4, 5.6 ml Milli-Q water) for 2 hours at room temperature or Mouse-On-Mouse Blocking Kit (Vector Laboratories, Inc, Burlingame, CA) and stained with primary antibodies (**Supplemental Table 2**) diluted in antibody diluent (10 ml overnight at 4°C). Slides were then washed in TBST and incubated with secondary antibodies for 2 hours at room temperature. Slides were counter stained with Hoechst 33342 nuclear stain (Supplemental Table 1) for 5 minutes, washed in TBST, and mounted using ProLong Glass Antifade Mountant (Invitrogen, Carlsbad, CA) and #1.5 Slip-Rite cover glass (Richard-Allan Scientific, San Diego, California). Images were acquired using a Leica TCS SP8 microscope using the Leica LAS X software (Wetzlar, Germany). A White Light Laser with 20x objective (air) was used to capture full section tiled images, 20x magnification images, and 3.15x optical zoom images of regions of interest equivalent to 63x magnification.

Image Quantification

High resolution 20x lens, 3.15x zoom, images were counted by skilled operator for cell number quantification (*Hoxa11-CreER^{T2};ROSA-TdTomato* n=2 mice/antigen of interest, n=3 regions of interest/mouse). Hoechst 33342

stained channel nuclei were first counted to select whole cells within the image frame. Number of *Hoxa11*- lineage and antigen of interest expressing cells were counted for quantification. Mean and standard error was calculated, and graphs were created in GraphPad Prism 8 (GSL Biotech LLC, Chicago, IL).

Supplemental References

Arroyo, E.J., Xu, T., Poliak, S., Watson, M., Peles, E., and Scherer, S.S. (2001). Internodal specializations of myelinated axons in the central nervous system. Cell Tissue Res *305*, 53-66.

Bergen, V., Lange, M., Peidli, S., Wolf, F.A., and Theis, F.J. (2020). Generalizing RNA velocity to transient cell states through dynamical modeling. Nat Biotechnol *38*, 1408-1414.

Bierie, B., Pierce, S.E., Kroeger, C., Stover, D.G., Pattabiraman, D.R., Thiru, P., Liu Donaher, J., Reinhardt, F., Chaffer, C.L., Keckesova, Z.*, et al.* (2017). Integrin-beta4 identifies cancer stem cell-enriched populations of partially mesenchymal carcinoma cells. Proc Natl Acad Sci U S A *114*, E2337-E2346.

Bondjers, C., He, L., Takemoto, M., Norlin, J., Asker, N., Hellstrom, M., Lindahl, P., and Betsholtz, C. (2006). Microarray analysis of blood microvessels from PDGF-B and PDGF-Rbeta mutant mice identifies novel markers for brain pericytes. FASEB J *20*, 1703-1705.

Butler, A., Hoffman, P., Smibert, P., Papalexi, E., and Satija, R. (2018). Integrating single-cell transcriptomic data across different conditions, technologies, and species. Nat Biotechnol *36*, 411-420.

Cao, J., Spielmann, M., Qiu, X., Huang, X., Ibrahim, D.M., Hill, A.J., Zhang, F., Mundlos, S., Christiansen, L., Steemers, F.J.*, et al.* (2019). The single-cell transcriptional landscape of mammalian organogenesis. Nature *566*, 496-502.

Cui, C., Bi, R., Liu, W., Guan, S., Li, P., Song, D., Xu, R., Zheng, L., Yuan, Q., Zhou, X.*, et al.* (2020). Role of PTH1R Signaling in Prx1(+) Mesenchymal Progenitors during Eruption. J Dent Res *99*, 1296-1305.

Davis, M.R., Andersson, R., Severin, J., de Hoon, M., Bertin, N., Baillie, J.K., Kawaji, H., Sandelin, A., Forrest, A.R., Summers, K.M.*, et al.* (2014). Transcriptional profiling of the human fibrillin/LTBP gene family, key regulators of mesenchymal cell functions. Mol Genet Metab *112*, 73-83.

Diederichs, S., Tonnier, V., Marz, M., Dreher, S.I., Geisbusch, A., and Richter, W. (2019). Regulation of WNT5A and WNT11 during MSC in vitro chondrogenesis: WNT inhibition lowers BMP and hedgehog activity, and reduces hypertrophy. Cell Mol Life Sci *76*, 3875-3889.

Docheva, D., Hunziker, E.B., Fassler, R., and Brandau, O. (2005). Tenomodulin is necessary for tenocyte proliferation and tendon maturation. Mol Cell Biol *25*, 699-705.

Drev, D., Harpain, F., Beer, A., Stift, A., Gruber, E.S., Klimpfinger, M., Thalhammer, S., Reti, A., Kenner, L., Bergmann, M.*, et al.* (2019). Impact of Fibroblast-Derived SPARC on Invasiveness of Colorectal Cancer Cells. Cancers (Basel) *11*.

Drummond, R.A., Swamydas, M., Oikonomou, V., Zhai, B., Dambuza, I.M., Schaefer, B.C., Bohrer, A.C., Mayer-Barber, K.D., Lira, S.A., Iwakura, Y.*, et al.* (2019). CARD9(+) microglia promote antifungal immunity via IL-1beta- and CXCL1-mediated neutrophil recruitment. Nat Immunol *20*, 559-570.

Fan, X., Waardenberg, A.J., Demuth, M., Osteil, P., Sun, J.Q.J., Loebel, D.A.F., Graham, M., Tam, P.P.L., and Fossat, N. (2020). TWIST1 Homodimers and Heterodimers Orchestrate Lineage-Specific Differentiation. Mol Cell Biol *40*.

Fernandez, I.Z., Baxter, R.M., Garcia-Perez, J.E., Vendrame, E., Ranganath, T., Kong, D.S., Lundquist, K., Nguyen, T., Ogolla, S., Black, J.*, et al.* (2019). A novel human IL2RB mutation results in T and NK cell-driven immune dysregulation. J Exp Med *216*, 1255-1267.
Fujiwara, S., Hoshikawa, S., Ueno, T., Hirata, M., Saito, T., Ikeda, T., Kawaguchi, H., Nakamura, K., Tanaka, S., and Ogata, T. (2014). SOX10 transactivates S100B to suppress Schwann cell proliferation and to promote myelination. PLoS One *9*, e115400.
Gordon, S., and Martinez, F.O. (2010). Alternative activation of macrophages: mechanism and functions. Immunity *32*, 593-604.
Herster, F., Bittner, Z., Archer, N.K., Dickhofer, S., Eisel, D., Eigenbrod, T., Knorpp, T., Schneiderhan-Marra, N., Loffler, M.W., Kalbacher, H.*, et al.* (2020). Neutrophil extracellular trap-associated RNA and LL37 enable self-amplifying inflammation in psoriasis. Nat Commun *11*, 105.
Hou, Z., Wang, X., Cai, J., Zhang, J., Hassan, A., Auer, M., and Shi, X. (2018). Platelet-Derived Growth Factor Subunit B Signaling Promotes Pericyte Migration in Response to Loud Sound in the Cochlear Stria Vascularis. J Assoc Res Otolaryngol *19*, 363-379.
Huang, A.H., Watson, S.S., Wang, L., Baker, B.M., Akiyama, H., Brigande, J.V., and Schweitzer, R. (2019). Requirement for scleraxis in the recruitment of mesenchymal progenitors during embryonic tendon elongation. Development *146*.
Hwang, C., Marini, S., Huber, A.K., Stepien, D.M., Sorkin, M., Loder, S., Pagani, C.A., Li, J., Visser, N.D., Vasquez, K.*, et al.* (2019). Mesenchymal VEGFA induces aberrant differentiation in heterotopic ossification. Bone Res *7*, 36.
Karkkainen, M.J., Haiko, P., Sainio, K., Partanen, J., Taipale, J., Petrova, T.V., Jeltsch, M., Jackson, D.G., Talikka, M., Rauvala, H.*, et al.* (2004). Vascular endothelial growth factor C is required for sprouting of the first lymphatic vessels from embryonic veins. Nat Immunol *5*, 74-80.
La Manno, G., Soldatov, R., Zeisel, A., Braun, E., Hochgerner, H., Petukhov, V., Lidschreiber, K., Kastriti, M.E., Lonnerberg, P., Furlan, A.*, et al.* (2018). RNA velocity of single cells. Nature *560*, 494-498.
Lee, H., Lee, Y.J., Choi, H., Seok, J.W., Yoon, B.K., Kim, D., Han, J.Y., Lee, Y., Kim, H.J., and Kim, J.W. (2017). SCARA5 plays a critical role in the commitment of mesenchymal stem cells to adipogenesis. Sci Rep *7*, 14833.
Li, M., Wang, J., Wang, C., Xia, L., Xu, J., Xie, X., and Lu, W. (2020). Microenvironment remodeled by tumor and stromal cells elevates fibroblast-derived COL1A1 and facilitates ovarian cancer metastasis. Exp Cell Res *394*, 112153.
Lilla, J.N., Chen, C.C., Mukai, K., BenBarak, M.J., Franco, C.B., Kalesnikoff, J., Yu, M., Tsai, M., Piliponsky, A.M., and Galli, S.J. (2011). Reduced mast cell and basophil numbers and function in Cpa3-Cre; Mcl-1fl/fl mice. Blood *118*, 6930-6938.
Liu, L.L., Landskron, J., Ask, E.H., Enqvist, M., Sohlberg, E., Traherne, J.A., Hammer, Q., Goodridge, J.P., Larsson, S., Jayaraman, J.*, et al.* (2016). Critical Role of CD2 Co-stimulation in Adaptive Natural Killer Cell Responses Revealed in NKG2C-Deficient Humans. Cell Rep *15*, 1088-1099.
Liu, Y., Lyle, S., Yang, Z., and Cotsarelis, G. (2003). Keratin 15 promoter targets putative epithelial stem cells in the hair follicle bulge. J Invest Dermatol *121*, 963-968.
Loder, S.J., Agarwal, S., Chung, M.T., Cholok, D., Hwang, C., Visser, N., Vasquez, K., Sorkin, M., Habbouche, J., Sung, H.H.*, et al.* (2018). Characterizing the Circulating Cell Populations in Traumatic Heterotopic Ossification. Am J Pathol *188*, 2464-2473.

Matsui, T., Hayashi-Kisumi, F., Kinoshita, Y., Katahira, S., Morita, K., Miyachi, Y., Ono, Y., Imai, T., Tanigawa, Y., Komiya, T.*, et al.* (2004). Identification of novel keratinocyte-secreted peptides dermokine-alpha/-beta and a new stratified epithelium-secreted protein gene complex on human chromosome 19q13.1. Genomics *84*, 384-397.
Mitsialis, V., Wall, S., Liu, P., Ordovas-Montanes, J., Parmet, T., Vukovic, M., Spencer, D., Field, M., McCourt, C., Toothaker, J.*, et al.* (2020). Single-Cell Analyses of Colon and Blood Reveal Distinct Immune Cell Signatures of Ulcerative Colitis and Crohn's Disease. Gastroenterology *159*, 591-608 e510.
Morikawa, S., Mabuchi, Y., Kubota, Y., Nagai, Y., Niibe, K., Hiratsu, E., Suzuki, S., Miyauchi-Hara, C., Nagoshi, N., Sunabori, T.*, et al.* (2009). Prospective identification, isolation, and systemic transplantation of multipotent mesenchymal stem cells in murine bone marrow. J Exp Med *206*, 2483-2496.
Noack, S., Seiffart, V., Willbold, E., Laggies, S., Winkel, A., Shahab-Osterloh, S., Florkemeier, T., Hertwig, F., Steinhoff, C., Nuber, U.A.*, et al.* (2014). Periostin secreted by mesenchymal stem cells supports tendon formation in an ectopic mouse model. Stem Cells Dev *23*, 1844-1857.
Nywening, T.M., Belt, B.A., Cullinan, D.R., Panni, R.Z., Han, B.J., Sanford, D.E., Jacobs, R.C., Ye, J., Patel, A.A., Gillanders, W.E.*, et al.* (2018). Targeting both tumour-associated CXCR2(+) neutrophils and CCR2(+) macrophages disrupts myeloid recruitment and improves chemotherapeutic responses in pancreatic ductal adenocarcinoma. Gut *67*, 1112-1123.
Ono, N., Ono, W., Nagasawa, T., and Kronenberg, H.M. (2014). A subset of chondrogenic cells provides early mesenchymal progenitors in growing bones. Nat Cell Biol *16*, 1157-1167.
Park, S., Sorenson, C.M., and Sheibani, N. (2015). PECAM-1 isoforms, eNOS and endoglin axis in regulation of angiogenesis. Clin Sci (Lond) *129*, 217-234.
Paulin, D., and Li, Z. (2004). Desmin: a major intermediate filament protein essential for the structural integrity and function of muscle. Exp Cell Res *301*, 1-7.
Perez-Zsolt, D., Martinez-Picado, J., and Izquierdo-Useros, N. (2019). When Dendritic Cells Go Viral: The Role of Siglec-1 in Host Defense and Dissemination of Enveloped Viruses. Viruses *12*.
Rabinowich, H., Pricop, L., Herberman, R.B., and Whiteside, T.L. (1994). Expression and function of CD7 molecule on human natural killer cells. J Immunol *152*, 517-526.
Ramirez, F., Ryan, D.P., Gruning, B., Bhardwaj, V., Kilpert, F., Richter, A.S., Heyne, S., Dundar, F., and Manke, T. (2016). deepTools2: a next generation web server for deep-sequencing data analysis. Nucleic Acids Res *44*, W160-165.
Ray, H.C., Corliss, B.A., Bruce, A.C., Kesting, S., Dey, P., Mansour, J., Seaman, S.A., Smolko, C.M., Mathews, C., Dey, B.K.*, et al.* (2020). Myh11+ microvascular mural cells and derived mesenchymal stem cells promote retinal fibrosis. Sci Rep *10*, 15808.
Roberts, M.D., Romero, M.A., Mobley, C.B., Mumford, P.W., Roberson, P.A., Haun, C.T., Vann, C.G., Osburn, S.C., Holmes, H.H., Greer, R.A.*, et al.* (2018). Skeletal muscle mitochondrial volume and myozenin-1 protein differences exist between high versus low anabolic responders to resistance training. PeerJ *6*, e5338.
Ruhland, M.K., Roberts, E.W., Cai, E., Mujal, A.M., Marchuk, K., Beppler, C., Nam, D., Serwas, N.K., Binnewies, M., and Krummel, M.F. (2020). Visualizing Synaptic Transfer of Tumor Antigens among Dendritic Cells. Cancer Cell *37*, 786-799 e785.
Sambasivan, R., Yao, R., Kissenpfennig, A., Van Wittenberghe, L., Paldi, A., Gayraud-Morel, B., Guenou, H., Malissen, B., Tajbakhsh, S., and Galy, A. (2011). Pax7-expressing satellite cells are indispensable for adult skeletal muscle regeneration. Development *138*, 3647-3656.

Schmidt, M., Micke, P., Gehrmann, M., and Hengstler, J.G. (2012). Immunoglobulin kappa chain as an immunologic biomarker of prognosis and chemotherapy response in solid tumors. Oncoimmunology *1*, 1156-1158.
Sherr, C.J., Rettenmier, C.W., Sacca, R., Roussel, M.F., Look, A.T., and Stanley, E.R. (1985). The c-fms proto-oncogene product is related to the receptor for the mononuclear phagocyte growth factor, CSF-1. Cell *41*, 665-676.
Shy, M.E., Hobson, G., Jain, M., Boespflug-Tanguy, O., Garbern, J., Sperle, K., Li, W., Gow, A., Rodriguez, D., Bertini, E.*, et al.* (2003). Schwann cell expression of PLP1 but not DM20 is necessary to prevent neuropathy. Ann Neurol *53*, 354-365.
Smith, R.K., Zunino, L., Webbon, P.M., and Heinegard, D. (1997). The distribution of cartilage oligomeric matrix protein (COMP) in tendon and its variation with tendon site, age and load. Matrix Biol *16*, 255-271.
Sorkin, M., Huber, A.K., Hwang, C., Carson, W.F.t., Menon, R., Li, J., Vasquez, K., Pagani, C., Patel, N., Li, S.*, et al.* (2020). Regulation of heterotopic ossification by monocytes in a mouse model of aberrant wound healing. Nat Commun *11*, 722.
Sun, L., Clavijo, P.E., Robbins, Y., Patel, P., Friedman, J., Greene, S., Das, R., Silvin, C., Van Waes, C., Horn, L.A.*, et al.* (2019). Inhibiting myeloid-derived suppressor cell trafficking enhances T cell immunotherapy. JCI Insight *4*.
Sundaram, K., Nishimura, R., Senn, J., Youssef, R.F., London, S.D., and Reddy, S.V. (2007). RANK ligand signaling modulates the matrix metalloproteinase-9 gene expression during osteoclast differentiation. Exp Cell Res *313*, 168-178.
Tao, H., Berno, A.J., Cox, D.R., and Frazer, K.A. (2007). In vitro human keratinocyte migration rates are associated with SNPs in the KRT1 interval. PLoS One *2*, e697.
Tesone, A.J., Rutkowski, M.R., Brencicova, E., Svoronos, N., Perales-Puchalt, A., Stephen, T.L., Allegrezza, M.J., Payne, K.K., Nguyen, J.M., Wickramasinghe, J.*, et al.* (2016). Satb1 Overexpression Drives Tumor-Promoting Activities in Cancer-Associated Dendritic Cells. Cell Rep *14*, 1774-1786.
Tian, X., Zheng, Y., Yin, K., Ma, J., Tian, J., Zhang, Y., Mao, L., Xu, H., and Wang, S. (2020). LncRNA AK036396 Inhibits Maturation and Accelerates Immunosuppression of Polymorphonuclear Myeloid-Derived Suppressor Cells by Enhancing the Stability of Ficolin B. Cancer Immunol Res *8*, 565-577.
Trapnell, C., Cacchiarelli, D., Grimsby, J., Pokharel, P., Li, S., Morse, M., Lennon, N.J., Livak, K.J., Mikkelsen, T.S., and Rinn, J.L. (2014). The dynamics and regulators of cell fate decisions are revealed by pseudotemporal ordering of single cells. Nat Biotechnol *32*, 381-386.
Vanlandewijck, M., He, L., Mae, M.A., Andrae, J., Ando, K., Del Gaudio, F., Nahar, K., Lebouvier, T., Lavina, B., Gouveia, L.*, et al.* (2018). A molecular atlas of cell types and zonation in the brain vasculature. Nature *554*, 475-480.
Waddell, L.A., Lefevre, L., Bush, S.J., Raper, A., Young, R., Lisowski, Z.M., McCulloch, M.E.B., Muriuki, C., Sauter, K.A., Clark, E.L.*, et al.* (2018). ADGRE1 (EMR1, F4/80) Is a Rapidly-Evolving Gene Expressed in Mammalian Monocyte-Macrophages. Front Immunol *9*, 2246.
Wang, R., Zhang, M., Ou, Z., He, W., Chen, L., Zhang, J., He, Y., Xu, R., Jiang, S., Qi, L.*, et al.* (2019a). Long noncoding RNA DNM3OS promotes prostate stromal cells transformation via the miR-29a/29b/COL3A1 and miR-361/TGFbeta1 axes. Aging (Albany NY) *11*, 9442-9460.
Wang, X., Rojas-Quintero, J., Wilder, J., Tesfaigzi, Y., Zhang, D., and Owen, C.A. (2019b). Tissue Inhibitor of Metalloproteinase-1 Promotes Polymorphonuclear Neutrophil (PMN)

Pericellular Proteolysis by Anchoring Matrix Metalloproteinase-8 and -9 to PMN Surfaces. J Immunol *202*, 3267-3281.
Wigle, J.T., and Oliver, G. (1999). Prox1 function is required for the development of the murine lymphatic system. Cell *98*, 769-778.
Wragg, J.W., Finnity, J.P., Anderson, J.A., Ferguson, H.J., Porfiri, E., Bhatt, R.I., Murray, P.G., Heath, V.L., and Bicknell, R. (2016). MCAM and LAMA4 Are Highly Enriched in Tumor Blood Vessels of Renal Cell Carcinoma and Predict Patient Outcome. Cancer Res *76*, 2314-2326.
Yang, M., Birnbaum, M.J., MacKay, C.A., Mason-Savas, A., Thompson, B., and Odgren, P.R. (2008). Osteoclast stimulatory transmembrane protein (OC-STAMP), a novel protein induced by RANKL that promotes osteoclast differentiation. J Cell Physiol *215*, 497-505.
Zalmai, L., Viailly, P.J., Biichle, S., Cheok, M., Soret, L., Angelot-Delettre, F., Petrella, T., Collonge-Rame, M.A., Seilles, E., Geffroy, S.*, et al.* (2020). Plasmacytoid dendritic cells proliferation associated with acute myeloid leukemia: phenotype profile and mutation landscape. Haematologica *Online ahead of print*.
Zhou, B.O., Yue, R., Murphy, M.M., Peyer, J.G., and Morrison, S.J. (2014). Leptin-receptor-expressing mesenchymal stromal cells represent the main source of bone formed by adult bone marrow. Cell Stem Cell *15*, 154-168.
Zhou, Y., Bian, S., Zhou, X., Cui, Y., Wang, W., Wen, L., Guo, L., Fu, W., and Tang, F. (2020). Single-Cell Multiomics Sequencing Reveals Prevalent Genomic Alterations in Tumor Stromal Cells of Human Colorectal Cancer. Cancer Cell *38*, 818-828 e815.